View metadata, citation and similar papers at core.ac.uk
brought to you by CORE
provided by Sissa Digital Library

Published for SISSA by Springer

Received: September 3, 2018
Accepted: October 10, 2018
Published: October 15, 2018

Combined explanations of B-physics anomalies: the sterile neutrino solution

Aleksandr Azatov,[a,b] **Daniele Barducci,**[a,b] **Diptimoy Ghosh,**[b,c] **David Marzocca**[b] **and Lorenzo Ubaldi**[a,b]

[a] *SISSA International School for Advanced Studies, Via Bonomea 265, 34136, Trieste, Italy*
[b] *INFN — Sezione di Trieste, Via Bonomea 265, 34136, Trieste, Italy*
[c] *ICTP International Centre for Theoretical Physics, Strada Costiera 11, 34014 Trieste, Italy*

E-mail: aleksandr.azatov@sissa.it, daniele.barducci@sissa.it, dghosh@ictp.it, david.marzocca@ts.infn.it, lubaldi@sissa.it

Abstract: In this paper we provide a combined explanation of charged- and neutral-current B-physics anomalies assuming the presence of a light sterile neutrino N_R which contributes to the $B \to D^{(*)}\tau\nu$ processes. We focus in particular on two simplified models, where the mediator of the flavour anomalies is either a vector leptoquark $U_1^\mu \sim (\mathbf{3}, \mathbf{1}, 2/3)$ or a scalar leptoquark $S_1 \sim (\bar{\mathbf{3}}, \mathbf{1}, 1/3)$. We find that U_1^μ can successfully reproduce the required deviations from the Standard Model while being at the same time compatible with all other flavour and precision observables. The scalar leptoquark instead induces a tension between B_s mixing and the neutral-current anomalies. For both states we present the limits and future projections from direct searches at the LHC finding that, while at present both models are perfectly allowed, all the parameter space will be tested with more luminosity. Finally, we study in detail the cosmological constraints on the sterile neutrino N_R and the conditions under which it can be a candidate for dark matter.

Keywords: Phenomenological Models

ArXiv ePrint: 1807.10745

Open Access, © The Authors.
Article funded by SCOAP[3].

https://doi.org/10.1007/JHEP10(2018)092

JHEP10(2018)092

Contents

1 Introduction **1**

2 Simplified models and flavour observables **4**
- 2.1 Vector LQ U_1 4
- 2.2 Scalar LQ S_1 7

3 Collider searches **10**
- 3.1 Vector leptoquark U_1 10
- 3.2 Scalar LQ S_1 13

4 Neutrino masses and decays **15**
- 4.1 Addressing only $R(D^{(*)})$ 15
- 4.2 Addressing also $R(K^{(*)})$ 15

5 Cosmology of N_R **17**
- 5.1 Relic density 17
- 5.2 $\Delta N_{\rm eff}$ 18
- 5.3 The dark matter option and entropy injection 19

6 Conclusions **21**

A Boltzmann equation **23**

JHEP10(2018)092

1 Introduction

Various intriguing hints of New Physics (NP) have been reported in the last years in the form of lepton flavour universality (LFU) violations in semileptonic B decays. In particular the $R(D^{(*)}) = \mathcal{B}(B \to D^{(*)}\tau\nu)/\mathcal{B}(B \to D^{(*)}\ell\nu)$ observable in $b \to c\tau\nu$ charged current transition, with $\ell = e, \mu$, has been measured by the BaBar [1, 2], Belle [3–5] and LHCb [6–8] collaborations to be consistently above the Standard Model (SM) predictions. Once global fits are performed [9, 10], the combined statistical significance of the anomaly is just above the $\sim 4\sigma$ level. Other deviations from the SM have been observed in the LFU ratios of neutral-current B decays, $R(K^{(*)}) = \mathcal{B}(B \to K^{(*)}\mu^+\mu^-)/\mathcal{B}(B \to K^{(*)}e^+e^-)$ [11, 12]. Also in this case the overall significance is around 4σ. This discrepancy, if interpreted as due to some NP contribution in the $b \to s\ell\bar{\ell}$ transition, is further corroborated by another deviation measured in the angular distributions of the process $B \to K^*\mu^+\mu^-$ [13, 14], for which however SM theoretical predictions are less under control.

Finding a combined explanation for both anomalies in terms of some Beyond the SM (BSM) physics faces various challenges. In particular, in the SM the $b \to c\tau\nu$ transition

occurs at tree-level and an explanation of the $R(D^{(*)})$ anomaly generally requires NP close to TeV scale, for which several constraints from direct searches for new states at collider experiments as well as in precision electroweak measurements and other flavour observables can be stringent, see e.g. refs. [15–41]. On the other hand, the neutral current $b \to s\ell^+\ell^-$ transition occurs in the SM through a loop-induced process, thus hinting to a higher NP scale or smaller couplings responsible for the $R(K^{(*)})$ anomaly.

Concerning the $R(D^{(*)})$ observables, it has recently been proposed that the measured enhancement with respect to the SM prediction can also be obtained by adding a new right-handed fermion, singlet under the SM gauge group, hereafter dubbed N_R [42, 43] (see also [26, 44–47] for earlier related studies). Differently from other explanations where the NP contributions directly enhance the $b \to c\tau\nu_\tau$ transition, this solution allows to evade the stringent constraints arising from the $\mathrm{SU}(2)_L$ doublet nature of the SM ν_τ neutrino. In this case the $B \to D^{(*)}\tau\nu$ decay rate becomes the sum of two non-interfering contributions: $\mathcal{B}(B \to D^{(*)}\tau\nu) = \mathcal{B}(B \to D^{(*)}\tau\nu_\tau) + \mathcal{B}(B \to D^{(*)}\tau N_R)$.

Several effective operators involving N_R can be written at the B-meson mass scale. In order to ensure that the differential distributions in the $B \to D^{(*)}\tau N_R$ process are compatible with the SM ones, as implicit in the global fits where the experimental acceptances are not assumed to be drastically modified by the presence of extra NP contributions, we assume that the sterile neutrino has a mass below $\sim \mathcal{O}(100)$ MeV [43] and that the dominant contributions to the $R(D^{(*)})$ anomaly is given by a right-right vector operator

$$\mathcal{L}_{BSM}^{b\to c\tau\nu} = \frac{c_{R_D}}{\Lambda^2}\,(\bar{c}_R\gamma_\mu b_R)\,(\bar{\tau}_R\gamma^\mu N_R) + h.c.\ . \tag{1.1}$$

Matching to the observed excess one finds [9] (Summer 2018 update [10])

$$R_{D^{(*)}} \equiv \frac{R(D)}{R(D)_{\rm SM}} = \frac{R(D^*)}{R(D^*)_{\rm SM}} = 1 + \left|\frac{c_{R_D}v^2}{2\Lambda^2 V_{cb}}\right|^2 = 1.218 \pm 0.052\,, \tag{1.2}$$

where $v \approx 246$ GeV is the vacuum expectation value of the SM Higgs field. This gives a NP scale required to fit the observed excess

$$\Lambda/\sqrt{c_{R_D}} = (1.27^{+0.09}_{-0.07})\ \ \text{TeV}\ . \tag{1.3}$$

Such a low NP scale strongly suggests that this operator could be generated by integrating out at tree-level some heavy mediator. There are only three possible new degrees of freedom which can do that:

- a charged vector $\quad W'_\mu \sim (\mathbf{1}, \mathbf{1}, +1)$,
- a vector leptoquark $\quad U_1^\mu \sim (\mathbf{3}, \mathbf{1}, +2/3)$,
- a scalar leptoquark $\quad S_1 \sim (\bar{\mathbf{3}}, \mathbf{1}, +1/3)$,

where in parentheses we indicate their $\mathrm{SU}(3)_c \times \mathrm{SU}(2)_L \times \mathrm{U}(1)_Y$ quantum numbers.[1] The case of the W'_μ has been recently studied in detail in refs. [42, 43]. In this work we focus

[1] We normalise the weak hypercharge as $Q = T^{3L} + Y$.

JHEP10(2018)092

on the two coulored leptoquark (LQ) models. Interestingly enough, both LQs can also contribute to the neutral-current $b \to s\mu^+\mu^-$ transition. In particular, the vector LQ U_1 contributes to that process at tree-level while the scalar S_1 only at one loop.

By considering the most general gauge invariant Lagrangians and assuming a specific flavour structure, we study in details the conditions under which the two LQ models can simultaneously explain both the $R(D^{(*)})$ and the $R(K^{(*)})$ measured values, taking into account all the relevant flavour and collider limits. Our findings show that the vector LQ provides a successful combined explanation of both anomalies, while being consistent with other low and high p_T experiments. Instead, while the scalar LQ can address $R(D^{(*)})$, a combined explanation of also $R(K^{(*)})$ is in tension with bounds arising from $B_s - \bar{B}_s$ mixing. Also, by studying the present limits and future projections for collider searches, we find that the Large Hadron Collider (LHC) will be able to completely test both models already with ~ 300 fb^{-1} of integrated luminosity.

For both models we then show that additional contributions to the mass of the active neutrinos generated by the operator responsible for reproducing the $R(K^{(*)})$ anomaly point to a specific extension of our framework, where neutrino masses are generated via the inverse see-saw mechanism [48–50]. We finally study the cosmological bounds on the right-handed neutrino N_R and discuss the conditions under which it can be identified with a Dark Matter (DM) candidate. We show that an $\mathcal{O}(1)$ keV sterile neutrino can behave as DM only when the operators responsible for the explanation of the $R(K^{(*)})$ anomaly are turned off. In this case N_R can reproduce the whole DM abundance observed in the Universe under the condition of additional entropy injection in the visible after the N_R decoupling, while being compatible with bounds arising from the presence of extra degrees of freedom in the early Universe and from structure formations at small scales.

Very recently, while this work was already in the final stages of preparation, ref. [51] appeared on the arXiv which has some overlap with our paper. In particular [51] also studies explanations of $R(D^{(*)})$ anomalies with the two LQs considered here, as well as with other states which generate operators different than the right-right one, and studies the present LHC limits from LQs pair production, with which we agree. In this work we go beyond that analysis by studying in detail the possibility of a *combined explanation* with the $b \to s\ell^+\ell^-$ neutral-current anomalies, by studying also LHC constraints from off-shell exchange of LQs, which turn out to be very relevant, by discussing a possible scenario that can account for the generation of neutrino masses and by presenting a detailed study of the cosmological aspects of the sterile neutrino relevant for the anomalies.

The layout of the paper is as follows. In section 2 we introduce the two LQ models with a right-handed neutrino and we describe their flavour structure and their implications for the relevant flavour observables. Limits arising from LHC searches are shown in section 3, while possible model extensions that can account for the generation of neutrino masses are discussed in section 4. Section 5 is dedicated to the discussion of the cosmological properties of N_R. We finally conclude in section 6.

JHEP10(2018)092

Operator	Definition	Coeff. U_1	Coeff. S_1
$(O^1_{lq})_{\alpha\beta ij}$	$(\bar{l}^\alpha_L\gamma_\mu l^\beta_L)(\bar{q}^i_L\gamma^\mu q^j_L)$	$2\xi\ g^q_{i\beta}g^{q*}_{j\alpha}$	$-\xi\ \lambda^{q*}_{i\alpha}\lambda^q_{j\beta}$
$(O^3_{lq})_{\alpha\beta ij}$	$(\bar{l}^\alpha_L\gamma_\mu\sigma^a l^\beta_L)(\bar{q}^i_L\gamma^\mu\sigma^a q^j_L)$	$2\xi\ g^q_{i\beta}g^{q*}_{j\alpha}$	$\xi\ \lambda^{q*}_{i\alpha}\lambda^q_{j\beta}$
$(O^1_{lequ})_{\alpha\beta ij}$	$(\bar{l}^\alpha_L e^\beta_R)\epsilon(\bar{q}^i_L u^j_R)$	0	$-2\xi\ \lambda^u_{j\beta}\lambda^{q*}_{i\alpha}$
$(O^3_{lequ})_{\alpha\beta ij}$	$(\bar{l}^\alpha_L\sigma_{\mu\nu}e^\beta_R)\epsilon(\bar{q}^i_L\sigma^{\mu\nu}u^j_R)$	0	$\frac{1}{2}\xi\ \lambda^u_{j\beta}\lambda^{q*}_{i\alpha}$
$(O_{eu})_{\alpha\beta ij}$	$(\bar{e}^\alpha_R\gamma_\mu e^\beta_R)(\bar{u}^i_R\gamma^\mu u^j_R)$	0	$-2\xi\ \lambda^{u\,*}_{i\alpha}\lambda^u_{j\beta}$
$(O_{ed})_{\alpha\beta ij}$	$(\bar{e}^\alpha_R\gamma_\mu e^\beta_R)(\bar{d}^i_R\gamma^\mu d^j_R)$	$4\xi g^d_{i\beta}g^{d*}_{j\alpha}$	0
$(O_{Nd})_{ij}$	$(\bar{N}_R\gamma_\mu N_R)(\bar{d}^i_R\gamma^\mu d^j_R)$	0	$-2\xi\ \lambda^{d*}_{iN}\lambda^d_{jN}$
$(O_{Nu})_{ij}$	$(\bar{N}_R\gamma_\mu N_R)(\bar{u}^i_R\gamma^\mu u^j_R)$	$4\xi g^u_{iN}g^{u*}_{jN}$	0
$(O_{eNud})_{\alpha ij}$	$(\bar{e}^\alpha_R\gamma_\mu N_R)(\bar{u}^i_R\gamma^\mu d^j_R)$	$4\xi g^{uN}_i g^{d*}_{j\alpha}$	$-2\xi\ \lambda^{u\,*}_{i\alpha}\lambda^d_j$
$(O^1_{lNqd})_{\alpha ij}$	$(\bar{l}^\alpha_L N_R)\epsilon(\bar{q}^i_L d^j_R)$	0	$-2\xi\ \lambda^d_{jN}\lambda^{q*}_{i\alpha}$
$(O^3_{lNqd})_{\alpha ij}$	$(\bar{l}^\alpha_L\sigma_{\mu\nu}N_R)\epsilon(\bar{q}^i_L\sigma^{\mu\nu}d^j_R)$	0	$\frac{1}{2}\xi\ \lambda^d_{jN}\lambda^{q*}_{i\alpha}$
$(O_{ledq})_{\alpha\beta ij}$	$(\bar{l}^\alpha_L e^\beta_R)(\bar{d}^i_R q^j_L)$	$-8\xi g^d_{i\beta}g^{q*}_{j\alpha}$	0
$(O_{lNuq})_{\alpha ij}$	$(\bar{l}^\alpha_L N_R)(\bar{u}^i_R q^j_L)$	$-8\xi g^u_{iN}g^{q*}_{j\alpha}$	0

Table 1. Dimension-six operators and corresponding Wilson coefficients obtained integrating out at tree-level the U_1 and S_1 mediators. $\xi = v^2/(4m^2_{U,S})$.

2 Simplified models and flavour observables

In this section we separately describe the interaction Lagrangians of the two candidate LQs, U_1 and S_1 in the presence of a right-handed SM singlet N_R, assuming baryon and lepton number conservation. We work in the down-quark and charged-lepton mass basis, so that $q^i_L = (V^*_{ji}u^j_L, d^i_L)^T$ and $\ell^\alpha_L = (\nu^\alpha_L, e^\alpha_L)^T$. Integrating out the LQs at the tree-level one generates a set of dimension-six operators, $\mathcal{L}^{\rm EFT} = -\frac{1}{v^2}\sum_x C_x O_x$, whose structures and corresponding value of the Wilson coefficients are indicated in table 1. For both mediators we study if the charged-current anomalies can be addressed while at the same time being consistent with all other experimental constraints. Furthermore, we also consider the possibility of addressing with the same mediators the neutral-current $R(K^{(*)})$ anomalies.

2.1 Vector LQ U_1

The general interaction Lagrangian of the vector LQ $U_1 \sim (\mathbf{3}, \mathbf{1}, +2/3)$ with SM fermions and a right-handed neutrino N_R reads

$$\mathcal{L} = U^\mu_1(\mathbf{g}^u_i\bar{u}^i_R\gamma_\mu N_R + \mathbf{g}^d_{i\alpha}\bar{d}^i_R\gamma_\mu e^\alpha_R + \mathbf{g}^q_{i\alpha}\bar{q}^i_L\gamma_\mu l^\alpha_L) + h.c.\,, \tag{2.1}$$

where $\mathbf{g}^{q,d}$ are 3×3 matrices while $\mathbf{g}^u$ is a 3-vector in flavour space. The integration of the U_1 state produces the seven dimension-six operators indicated in table 1, where $\xi = v^2/(4m^2_U)$. From these operators it is clear that this vector LQ can contribute to $R(D^{(*)})$ in several ways:

i) via the vector LL operator O^3_{lq} proportionally to $g^q_{b(s)\tau}$;

JHEP10(2018)092

ii) via the scalar operator O_{ledq} proportionally to $g^d_{b\tau} g^q_{b(s)\tau}$;

iii) via the scalar operator O_{lNuq} proportionally to $g^u_{cN} g^q_{b\tau}$;

iv) via the vector RR operator O_{eNud} proportionally to $g^u_{cN} g^d_{b\tau}$.

The first three solutions involve a large coupling to third-generation left-handed quarks and leptons and have been studied widely in the literature [30, 38, 52–60]. Such structures can potentially lead to some tension with Z boson couplings measurements, LFU tests in τ decays, and $B_s - \bar{B}_s$ mixing. To avoid these issues and since our goal is to study mediators contributing to $R(D^{(*)})$ mainly via the operator in eq. (1.1), we set $g^q_{i\tau} \approx 0$ and focus instead on case *iv)*. In order to explain both the $R(D^{(*)})$ and $R(K^{(*)})$ anomalies we assume the LQ couplings to fermions to have the following flavour structure:

$$\mathbf{g}^q = \begin{pmatrix} 0 & 0 & 0 \\ 0 & g^q_{s\mu} & 0 \\ 0 & g^q_{b\mu} & 0 \end{pmatrix}, \qquad \mathbf{g}^d = \begin{pmatrix} 0 & 0 & 0 \\ 0 & 0 & 0 \\ 0 & 0 & g^d_{b\tau} \end{pmatrix}, \qquad \mathbf{g}^u = (0,\ g^u_{cN}, 0)^T, \tag{2.2}$$

with $g^d_{b\tau} g^u_{cN} \sim \mathcal{O}(1)$, $g^q_{b\mu}, g^q_{s\mu} \ll 1$. Note that one could potentially also add a coupling to the right-handed top, but since it does not contribute to the flavour anomalies we neglect it in the following.

By fitting the excess in the charged-current LFU ratios one obtains with this coupling structure

$$\delta R_{D^{(*)}} = \frac{|g^{u\,*}_{cN} g^d_{b\tau}|^2}{m_U^4} \frac{v^4}{4|V_{cb}|^2} = 0.218 \pm 0.052 \tag{2.3}$$

hence

$$|g^u_{cN} g^d_{b\tau}| \sim 0.62 \sqrt{\frac{\delta R_{D^{(*)}}}{0.218}} \left(\frac{m_U}{1\ \text{TeV}}\right)^2. \tag{2.4}$$

With the couplings in eq. (2.2), the vector LQ also contributes at the tree-level to $b \to s\mu^+\mu^-$ transitions via the two operators $O^{1,3}_{lq}$. By fitting the anomaly and matching to the standard weak Hamiltonian notation we get

$$\Delta C^\mu_9 = -\Delta C^\mu_{10} = -\frac{\pi v^2}{\alpha V_{tb} V^*_{ts}} \frac{g^q_{b\mu} (g^q_{s\mu})^*}{m_U^2} = -0.61 \pm 0.12\,, \tag{2.5}$$

where we used the result of the global fit in [61] (see also [62–68]). This corresponds to

$$g^q_{b\mu} (g^q_{s\mu})^* = (-0.93 \pm 0.18) \times 10^{-3} \left(\frac{m_U}{1\ \text{TeV}}\right)^2. \tag{2.6}$$

The vector LQ, with the couplings required to fit the B-anomalies as detailed above, contributes also to other flavour and precision observables. While all constraints can be successfully satisfied, we list in the following the most relevant ones. The contribution to the $B_c \to \mu N$ decay width and the corresponding limit [69] are given by

$$\begin{aligned} \mathcal{B}(B_c \to \mu N) &= \frac{\tau_{B_c} f^2_{B_c} m_{B_c}}{64\pi} \left| \frac{c_{lNuq}}{\Lambda^2} \frac{m^2_{B_c}}{(\overline{m}_b + \overline{m}_c)} \right|^2 \lesssim 5(30)\% \\ &\to \quad |g^q_{b\mu} g^u_{cN}| \lesssim 0.23(0.57) \left(\frac{m_U}{1\ \text{TeV}}\right)^2, \end{aligned} \tag{2.7}$$

JHEP10(2018)092

where $f_{B_c} \approx 0.43$ GeV [70], $m_{B_c} \approx 6.275$ GeV and $\tau_{B_c} \approx 0.507 \times 10^{-12} s$ [71], and we use both the more aggressive and more conservative limits quoted in [69]. A chirally-enhanced contribution is also generated for the $D_s \to \mu N$ decay, which is measured at a few percent level [71]:

$$\mathcal{B}(D_s \to \mu\,\nu/N) = \frac{\tau_{D_s} f_{D_s}^2 m_{D_s}}{64\pi} \left(\frac{m_\mu^2}{(\Lambda_{\rm eff}^{cs})^4} + \left| \frac{2 g_{s\mu}^{q\,*} g_{cN}^u}{m_U^2} \frac{m_{D_s}^2}{(\overline{m}_s + \overline{m}_c)} \right|^2 \right) = (5.50 \pm 0.23) \times 10^{-3}\,, \tag{2.8}$$

where $\Lambda_{\rm eff}^{cs} = (1/2\sqrt{2} G_F V_{cs})^{1/2}$, $f_{D_s} \approx 0.25$ GeV [70], $m_{D_s} \approx 1.986$ GeV and $\tau_{D_s} \approx 5 \times 10^{-13} s$ [71], which gives an upper 95% CL bound $|g_{s\mu}^q g_{cN}^u| \lesssim 0.17 \left(\frac{m_U}{1\ \rm TeV}\right)^2$.

The prediction for the lepton flavour violating (LFV) decays $B_s \to \tau\mu$, $B \to K\tau\mu$, and $B \to K^*\tau\mu$ from the $(O_{ledq})_{\mu\tau bs}$ operator are given by [72]

$$\begin{aligned}
\mathcal{B}(B_s \to \tau\mu) &= \frac{\tau_{B_s} f_{B_s}^2 m_{B_s}}{32\pi} \left(1 - \frac{m_\tau^2}{m_{B_s}^2}\right)^2 \left| \frac{c_{ledq}}{\Lambda^2} \frac{m_{B_s}^2}{(\overline{m}_b + \overline{m}_s)} \right|^2 \\
&\approx 5.4 \times 10^{-5} \left| \frac{g_{s\mu}^{q\,*} g_{b\tau}^d}{10^{-2}} \left(\frac{1\ \rm TeV}{m_U}\right)^2 \right|^2 , \\
\mathcal{B}(B \to K^*\tau\mu) &\approx 1.6 \times 10^{-5} \left| \frac{g_{s\mu}^{q\,*} g_{b\tau}^d}{10^{-2}} \left(\frac{1\ \rm TeV}{m_U}\right)^2 \right|^2 , \\
\mathcal{B}(B \to K\tau\mu) &\approx 4.1 \times 10^{-5} \left| \frac{g_{s\mu}^{q\,*} g_{b\tau}^d}{10^{-2}} \left(\frac{1\ \rm TeV}{m_U}\right)^2 \right|^2 < 4.8 \times 10^{-5}
\end{aligned} \tag{2.9}$$

where $f_{B_s} \approx 0.224$ GeV [70], $m_{B_s} \approx 5.37$ GeV and $\tau_{B_s} \approx 1.51 \times 10^{-12} s$ [71]. In the last equation we also report the upper limit obtained by BaBar [73]. Future analyses by LHCb and Belle-II are expected to further improve the limits on these processes.

A contribution to $B_s - \bar{B}_s$ mixing is generated at the loop level and is proportional to $(g_{b\mu}^q (g_{s\mu}^q)^*)^2$, which makes it negligibly small given eq. (2.6). These couplings also induce a tree-level contribution to $b \to c\mu\nu$, which is constrained at the $\sim 1\%$ level, however also the prediction for this observable is well below the experimental bound due to the small size of the couplings.

Finally we notice that at one loop the vector LQ generates also contributions to Z couplings to SM fermions, precisely measured at LEP-1. These effects can also be understood from the renormalisation group (RG) evolution of the operators in table 1 from the scale m_U down to the electroweak scale [74–76]. The relevant deviations in Z couplings are:[2]

$$\begin{aligned}
|\Delta g_{\tau_R}^Z| &= \frac{v^2}{16\pi^2 m_U^2} \frac{g_Y^2 |g_{b\tau}^d|^2}{3} \log\frac{m_U}{m_Z} \approx (3.8 \times 10^{-5}) \frac{|g_{b\tau}^d|^2}{(m_U/1\ \rm TeV)^2} < 1.2 \times 10^{-3} \\
|\Delta g_{N_R}^Z| &= \frac{v^2}{32\pi^2 m_U^2} \frac{4 g_Y^2 |g_{cN}^u|^2}{3} \log\frac{m_U}{m_Z} \approx (7.5 \times 10^{-5}) \frac{|g_{cN}^u|^2}{(m_U/1\ \rm TeV)^2} < 2 \times 10^{-3}\,,
\end{aligned} \tag{2.10}$$

[2]Defined as $g_{f_{L,R}}^Z = g_{f_{L,R}}^{Z,\rm SM} + \Delta g_{f_{L,R}}^Z$, where $g_{f_{L,R}}^{Z,\rm SM} = (T_{3L}^f - Q^f s_{\theta_W}^2)$. The limit on $\Delta g_{\nu_R}^Z$ comes from $N_\nu = \Gamma_{inv}/\Gamma_{\nu\bar{\nu}}^{\rm SM} = 2 + \left|1 + 2\Delta g_{\nu_L^\mu}^Z\right|^2 + \left|2\Delta g_{\nu_R}^Z\right|^2 = 2.9840 \pm 0.0082$.

JHEP10(2018)092

where the 95% confidence level (CL) limits have been taken from ref. [77]. It is clear that the $\mathcal{O}(1)$ couplings required to address the $R(D^{(*)})$ anomalies do not induce any dangerous effects in these observables.

We conclude this section by stressing that the vector LQ U_1 with the coupling structure in eq. (2.2) is able to successfully fit both charged- and neutral-current B-physics anomalies, while at the same time satisfying all other flavour and precision constraints with no tuning required. In section 3 we show how this mediator can also pass all available limits from direct searches, but it should be observed with more data gathered at the LHC. Finally, in sections 4 and 5 we show how the sterile neutrino N_R can satisfy all constraints from both neutrino physics and cosmology.

2.2 Scalar LQ S_1

The general interaction Lagrangian for the scalar LQ $S_1 \sim (\bar{\mathbf{3}}, \mathbf{1}, +1/3)$ and a right-handed neutrino N_R is

$$\mathcal{L} = S_1 \left(\lambda^u_{i,\alpha} \bar{u}^{c,i}_R e^\alpha_R + \lambda^d_i \bar{d}^{c,i}_R N_R + \lambda^q_{i,\alpha} \bar{q}^{c,i}_L \epsilon \ell^\alpha_L \right) + \text{h.c.}\,, \tag{2.11}$$

where $\lambda^{q,u}$ are 3×3 matrices while λ^d is a 3-vector in flavour space and the supscript c denote the charge conjugation operator. The operators generated by integrating out this LQ are listed in table 1. As for the vector LQ, also the scalar can contribute to $R(D^{(*)})$ in several ways, including via a large coupling to third generation left-handed quarks and leptons [20, 24, 27, 31, 34, 35, 38, 78–84], which however leads to tension with electroweak precision tests and $B_s - \bar{B}_s$ mixing [38, 84]. We thus focus on the case where $g^q_{i\tau} \ll 1$ and where the leading contribution to $b \to c\tau\nu$ arises from the operator in eq. (1.1).

Contrary to the vector LQ, the scalar one does not contribute to $b \to s\mu^+\mu^-$ at the tree-level. It does, however, at one loop [20] via box diagrams proportionally to the $\lambda^q_{s\mu}\lambda^q_{b\mu}$ couplings. Our goal is thus to fit $R(D^{(*)})$ at tree-level via right-handed currents involving N_R, while possibly fitting $R(K^{(*)})$ at one-loop with the corresponding couplings to left-handed fermions. In this spirit we require the following couplings to be non-vanishing:

$$\lambda^q = \begin{pmatrix} 0 & 0 & 0 \\ 0 & \lambda^q_{s\mu} & 0 \\ 0 & \lambda^q_{b\mu} & 0 \end{pmatrix}, \qquad \lambda^u = \begin{pmatrix} 0 & 0 & 0 \\ 0 & 0 & \lambda^u_{c\tau} \\ 0 & 0 & 0 \end{pmatrix}, \qquad \lambda^d = \begin{pmatrix} 0, & 0, & \lambda^d_{bN} \end{pmatrix}^T . \tag{2.12}$$

In the limit where one does not address $R(K^{(*)})$, i.e. $\lambda^q_{q\mu} \approx 0$, the only NP contribution to $R(D^{(*)})$ is given by the operator in eq. (1.1):

$$\delta R_{D^{(*)}} = \frac{|\lambda^{u\,*}_{c\tau}\lambda^d_{bN}|^2}{4m_S^4} \frac{v^4}{4|V_{cb}|^2} = 0.218 \pm 0.052 \tag{2.13}$$

which further implies

$$|\lambda^u_{c\tau}\lambda^d_{bN}| \sim 1.25\sqrt{\frac{\delta R_{D^{(*)}}}{0.218}} \left(\frac{m_S}{1\ \text{TeV}}\right)^2 . \tag{2.14}$$

Thus with $\mathcal{O}(1)$ couplings also the scalar LQ should live at the TeV scale in order to explain the measured values of $R(D^{(*)})$. In the more general case, the couplings in λ^q in eq. (2.12)

JHEP10(2018)092

induce also different contributions to $R(D^{(*)})$ which can be relevant since, as shown below, $\lambda^q_{b\mu}$ should be large if one aims to fit $R(K^{(*)})$:

$$\begin{aligned} R_D = \frac{R(D)}{R(D)_{\rm SM}} &\approx 1 + 0.14|\lambda^u_{c\tau}\lambda^d_{bN}|^2 \left(\frac{m_S}{1\ \text{TeV}}\right)^{-4} + 0.19|\lambda^u_{c\tau}\lambda^q_{b\mu}|^2 \left(\frac{m_S}{1\ \text{TeV}}\right)^{-4} \\ &= 1.36 \pm 0.15\,, \\ R_{D^*} = \frac{R(D^*)}{R(D^*)_{\rm SM}} &\approx 1 + 0.14|\lambda^u_{c\tau}\lambda^d_{bN}|^2 \left(\frac{m_S}{1\ \text{TeV}}\right)^{-4} + 0.032|\lambda^u_{c\tau}\lambda^q_{b\mu}|^2 \left(\frac{m_S}{1\ \text{TeV}}\right)^{-4} \\ &= 1.186 \pm 0.062\,, \end{aligned} \tag{2.15}$$

with a correlation -0.203. The operator $\propto \lambda^u_{c\tau}\lambda^{q\,*}_{b\mu}(\bar\nu^\mu_L\tau_R)(\bar b_L c_R)$ also induces a chirally enhanced contribution to the LFV process $B_c \to \tau\bar\nu^\mu_L$, which can be constrained using LEP data to have at most a $\sim 10\%$ branching fraction [85]:

$$\mathcal{B}(B_c \to \tau\bar\nu^\mu_L) = \frac{\tau_{B_c} f^2_{B_c} m_{B_c}}{64\pi}\left(1 - \frac{m^2_\tau}{m^2_{B_c}}\right)^2 \left|\frac{\lambda^u_{c\tau}\lambda^q_{b\mu}}{2m^2_S}\frac{m^2_{B_c}}{(\overline{m}_b + \overline{m}_c)}\right|^2 \lesssim 10\%\ . \tag{2.16}$$

The corresponding constraint is

$$|\lambda^u_{c\tau}\lambda^q_{b\mu}| \lesssim 1.4\left(\frac{m_S}{1\ \text{TeV}}\right)^2\ , \tag{2.17}$$

which makes this contribution negligible for R_{D^*} but possibly relevant for R_D, eq. (2.15).

The couplings to quark and lepton doublets $\lambda^q_{q\mu}$ generate a $b \to c\mu\nu$ charged-current transition, which implies a violation of LFU in $b \to c\ell\nu$ processes which is however constrained at the percent level [86]

$$\delta R^{\mu e}_{b\to c} \approx 0.03\left(\frac{1\ \text{TeV}}{m_S}\right)^2 \text{Re}\left[\lambda^{q\,*}_{b\mu}\left(\lambda^q_{b\mu} + V_{cs}\frac{\lambda^q_{s\mu}}{V_{cb}}\right)\right] < \mathcal{O}(1\%). \tag{2.18}$$

Since, as shown below, in order to fit $R(K^{(*)})$ the coupling $\lambda^{q\,*}_{b\mu}$ has to be larger than 1, it is necessary to tune the parenthesis as

$$\lambda^q_{s\mu} \sim -\frac{V_{cb}}{V_{cs}}\lambda^q_{b\mu}\ . \tag{2.19}$$

This relation also suppresses the non-interfering contribution to the same observable from the $(O^{1,3}_{lNqd})_{\mu cb}$ operators. Note that this relation corresponds to aligning the coupling to $t_L\mu_L$ in the up-quark mass basis, so that the LQ has a much suppressed coupling to c_L. The same couplings also induce a possibly large tree-level contribution to $b \to s\nu^\mu_L\nu^\mu_L$. The 95% CL limit on $\mathcal{B}(B \to K^*\nu\nu)$ fixes the upper bound

$$R_{\nu\nu}:\quad -1.2\left(\frac{m_S}{1\ \text{TeV}}\right)^2 < \frac{\lambda^q_{b\mu}\lambda^{q\,*}_{s\mu}}{V_{tb}V^*_{ts}} < 2.2\left(\frac{m_S}{1\ \text{TeV}}\right)^2 \quad\longrightarrow\quad |\lambda^q_{b\mu}|^2 \lesssim 2.2\left(\frac{m_S}{1\ \text{TeV}}\right)^2\ , \tag{2.20}$$

where in the second step we used the condition in eq. (2.19).

JHEP10(2018)092

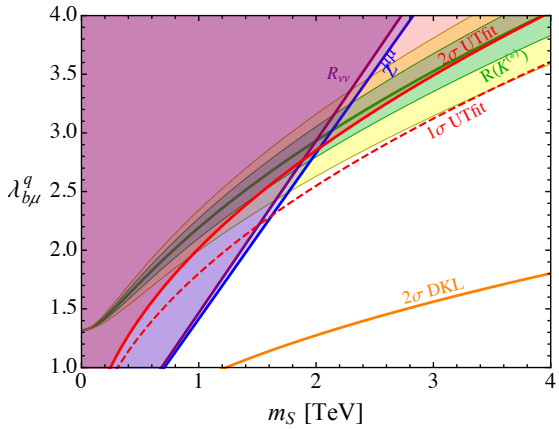

Figure 1. 95% CL limits from flavour observables and Z couplings measurements on $\lambda^q_{b\mu}$ as a function of the scalar LQ mass. The green (yellow) region represents the parameter space which fits $R(K^{(*)})$ at 1σ (2σ).

The loop contribution to $B \to K^{(*)}\mu^+\mu^-$ is given by [20]

$$\begin{aligned}\Delta C_9^\mu = -\Delta C_{10}^\mu &\approx \frac{m_t^2}{16\pi\alpha m_S^2}|V^*_{td_i}\lambda^q_{d_i\mu}|^2 - \frac{\sqrt{2}}{128\pi\alpha G_f m_S^2}\left(\frac{\lambda^q_{b\mu}\lambda^{q*}_{s\mu}}{V_{tb}V^*_{ts}}\right)|V^*_{td_i}\lambda^q_{d_i\mu}|^2 \\ &= -0.61 \pm 0.12 \end{aligned} \tag{2.21}$$

Imposing the condition of eq. (2.19) we obtain

$$|\lambda^q_{b\mu}|^2 \approx 0.87 + 3.84\left(\frac{m_S}{1\text{ TeV}}\right)\sqrt{\frac{\Delta C_9^\mu}{-0.61}}. \tag{2.22}$$

Hence an $\mathcal{O}(1)$ $\lambda^q_{b\mu}$ coupling is needed to explain the $R(K^{(*)})$ anomaly. This is compatible with the constraint in eq. (2.20) for $m_S \gtrsim 2$ TeV.

As for the case of the vector LQ, the RG evolution of the effective operators down to the electroweak scale generates an effect in Z couplings. In this setup this is particularly relevant for the $Z\mu\mu$ one, due to the contribution proportional to y_t^2:

$$\begin{aligned}\Delta g^Z_{\mu_L} &= \frac{v^2}{64\pi^2 m_S^2}\left(6y_t^2 + \frac{g_Y^2}{3} - g^2\right)|\lambda^q_{b\mu}|^2 \log\frac{m_S}{m_Z} \\ &\approx (1.1\times 10^{-3})\frac{|\lambda^q_{b\mu}|^2}{(m_S/1\text{ TeV})^2} < 2.2\times 10^{-3},\end{aligned} \tag{2.23}$$

which is compatible with eq. (2.22) for $m_S \gtrsim 2.2$ TeV. The effects in $Z\tau_R\tau_R$ and ZN_RN_R are similar to those in eq. (2.10) and do not pose relevant constraints.

At one loop, the couplings $\lambda^q_{b\mu}$ and $\lambda^q_{s\mu}$ also contribute to $B_s - \bar{B}_s$ mixing:

$$\frac{C_0^{\rm NP}}{C_0^{\rm SM}} = \frac{1}{C_0^{\rm SM}}\frac{v^2}{4m_S^2}\left(\frac{\lambda^q_{b\mu}\lambda^{q*}_{s\mu}}{V_{tb}V^*_{ts}}\right)^2 \approx 0.24\left(\frac{1\text{ TeV}}{m_S}\right)^2\left|\frac{\lambda^q_{b\mu}}{2}\right|^4 = \begin{cases} 0.07\pm 0.09 & \text{— UTfit [87]} \\ -0.11\pm 0.06 & \text{— DKL [88]}\end{cases}, \tag{2.24}$$

JHEP10(2018)092

where $C_0^{\rm SM} = 4\pi\alpha S_0(x_t)/s_w^2 \approx 1$. It is clear that some tension is present with the value required to fit $R(K^{(*)})$, eq. (2.22), for any value of m_S. These limits are shown in figure 1. While the model is compatible with the experimental bounds on B_s mixing within 2σ if the result from UTfit [87] is considered, the bound from ref. [88] (see also refs. [89, 90]) excludes the $R(K^{(*)})$ solution, unless some other NP contribution to $B_s - \bar{B}_s$ mixing cancels the one from S_1.

3 Collider searches

In section 2 we have shown that in order to explain the observed value of $R(D^{(*)})$ both the vector and the scalar LQ should have a mass that, for $\mathcal{O}(1)$ value of the couplings, are around 1 TeV, thus implying the possibility of testing their existence in high-energy collider experiments. At the LHC LQs can be searched for in three main ways: *i)* they can be produced on-shell via QCD interactions; *ii)* they can be singly produced via their couplings to SM fermions; *iii)* they can be exchanged in the t-channel in $q\bar{q}$ scattering.

In this section we will illustrate the main constraints arising from LHC searches on the two considered LQ models from both pair-production and off-shell exchange. Single-production modes, instead, while will be relevant in the future for large LQ masses, at present do not offer competitive bounds, see e.g. ref. [91].

3.1 Vector leptoquark U_1

Pair-production. The interactions of eq. (2.1) can be constrained in several ways by LHC searches. When produced on-shell and in pairs through QCD interactions, the LQs phenomenology is only dictated by the relative weight of their branching ratios. As we discussed in section 2, the couplings $g^q_{s\mu}$ and $g^q_{b\mu}$ in eq. (2.1) can give $R(K^{(*)})$ at tree-level, thus implying that they should be considerably smaller than $g^d_{b\tau}$ and g^u_{cN}, which are responsible for explaining $R(D^{(*)})$ also at tree-level, see eq. (2.6) and eq. (2.4). For this reason $g^q_{s\mu}$ and $g^q_{b\mu}$ can be neglected while studying the LHC phenomenology of the vector LQ. The relative rate of the dominant decay channels is thus set by the following ratio

$$\frac{\Gamma(U_1 \to b\bar{\tau})}{\Gamma(U_1 \to c\bar{N}_R)} \sim \frac{|g^d_{b\tau}|^2}{|g^u_{cN}|^2}. \tag{3.1}$$

Regarding production, LQs can be copiously produced in pairs at the LHC through QCD interactions described by the following Lagrangian

$$\mathcal{L}^{U_1}_{\rm kin.} = -\frac{1}{2} U^\dagger_{1\,\mu\nu} U_1^{\mu\nu} - i g_s \kappa U_1^{\mu\,\dagger} T^a U_1^\nu G^a_{\mu\nu} + m_U^2 U^\dagger_{1\,\mu} U_1^\mu. \tag{3.2}$$

Here g_s is the strong coupling constant, $G^a_{\mu\nu}$ the gluon field strength tensor, T^a the $\mathrm{SU}(3)_c$ generators with $a = 1, \ldots, 8$ and κ is a dimensionless parameter that depends on the ultra-violet origin of the vector LQ. The choices $\kappa = 0, 1$ correspond to the minimal coupling case and the Yang-Mills case respectively. Barring the choice of κ, the cross-section only depends on the LQ mass.[3] For our analysis we compute the LQ pair production cross-section at

[3] In reality, additional model dependent processes can contribute to the LQ pair production cross section. We however checked that for perturbative values of the LQ couplings they are subdominant with respect to leading QCD ones. This is also true for the case of the scalar LQ discussed in section 3.2.

JHEP10(2018)092

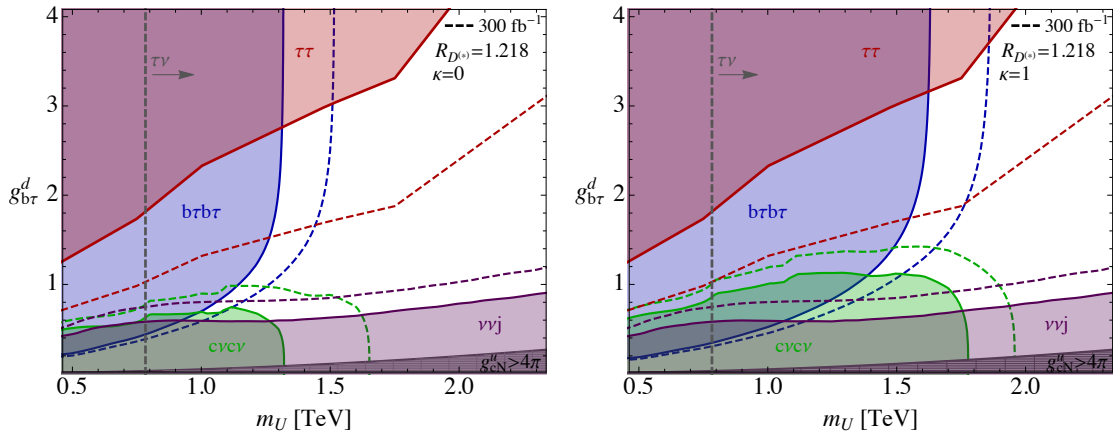

Figure 2. Limits arising from direct and indirect LHC searches in the $m_U - g^d_{b\tau}$ plane, with g^u_{cN} fixed to fit the central value of $R_{D^{(*)}}$ for $\kappa = 0$ (left) and $\kappa = 1$ (right). Current limits are shown as shaded areas, while projections for 300 fb^{-1} of integrated luminosity as dashed lines. The arrow indicates the region excluded by the $\tau\nu$ search. The region where g^u_{cN} becomes non perturbative is also illustrated.

LO in QCD with `MadGraph5_aMC@NLO` [92] through the implementation of the Lagrangian of eq. (3.2) in `Feynrules` performed in [91] that has been made publicly available.[4]

The CMS collaboration has performed various analyses targeting pair produced LQs. In particular the analysis in [94], recently updated in [95], searched for a pair of LQs decaying into a $2b2\tau$ final state setting a limit of ~ 5 fb on the inclusive cross-section times the branching ratio for a LQ with a mass of 1 TeV. In the case of the $2c2N_R$ final state, we can reinterpret the existing experiental limits on first and second generation squarks decaying into a light jet and a massless neutralino [96], for which the ATLAS collaboration provided the upper limits on the cross-sections for various squark masses on `HEPData`, which have then been used to compute the bounds as a function of the LQ mass.[5]

The bounds arising from LQs pair production searches are shown as green and blue shaded areas in figure 2 for $\kappa = 0$ (left panel) and 1 (right panel) in the $m_U - g^d_{b\tau}$ plane. Here g^u_{cN} has been fixed to match the central value of $R(D^{(*)})$ according to eq. (2.4). Also shown are the projections for a LHC integrated luminosity of 300 fb^{-1}, which have been obtained by rescaling the current limits on the cross section by the factor $\sqrt{300\ \text{fb}^{-1}/\mathcal{L}_0}$, with $\mathcal{L}_0$ the current luminosity of the considered analysis. All together we see that current direct searches are able to constrain vector LQs up to ~ 1.3 TeV for $\kappa = 0$, and ~ 1.8 TeV for $\kappa = 1$ when the dominant decay mode is into a $2c2N_R$ final state, with slightly weaker limits in the case of an inclusive $2b2\tau$ decay.

Off-shell exchange. From the Lagrangian of eq. (2.1), and with the assumptions of eq. (2.2), we see that other relevant constraints can arise from $\bar{c}c \to N_R N_R$, $\bar{b}b \to \tau\tau$ and

[4]Unless explicitely stated otherwise, all the cross-sections used in this work have been computed with `MadGraph5_aMC@NLO`. When the relevant model files were not publicly available, we have implemented the relevant Lagrangians with the `FeynRules` package and exported in the `UFO` format [93].

[5]The limits derived in this way agree with those obtained by the CMS collaboration by reinterpreting SUSY searches in [97].

JHEP10(2018)092

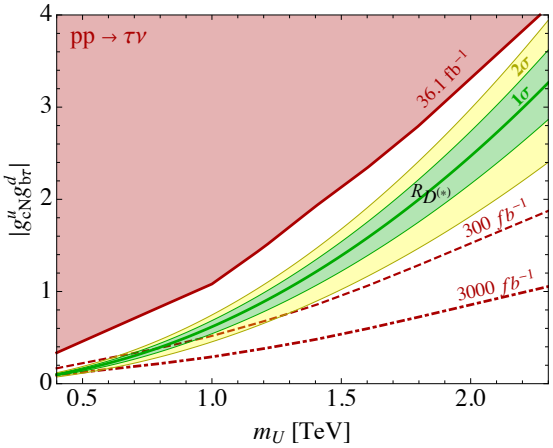

Figure 3. Present and projected limits from $\tau\nu$ searches in the $m_U - |g^u_{cN} g^d_{b\tau}|$ plane. Also shown are the 68% and 95% CL intervals around the central values of $R_{D^{(*)}}$, eq. (1.2).

$\bar{b}c \to \bar{\tau} N_R$ processes which occur through the exchange of a t-channel LQ.

In particular, $\bar{b}c \to \bar{\tau} N_R$ directly tests the same interactions responsible for explaining the $R(D^{(*)})$ anomalies. The ATLAS collaboration published a search for high-mass resonances in the $\tau\nu$ final state with 36 fb^{-1} of luminosity [98], which we can use to obtain limits in our model. To do this, we computed with `MadGraph5_aMC@NLO` the fiducial acceptance $\mathcal{A}$ and reconstruction efficiency ϵ in our model as a function of the threshold in the transverse mass m_T, and used the model-independent bound on $\sigma(pp \to \tau\nu + X) \times \mathcal{A} \times \epsilon$ as a function of m_T published in [98] to derive the constraints. We then rescale the expected limits on the cross section with the square root of the luminosity to derive the estimate for future projections. The present and future-projected limits in the m_U vs. $|g^u_{cN} g^d_{b\tau}|$ plane derived in this way are shown in figure 3, together with the band showing the region which fits the $R(D^{(*)})$ anomaly. We notice that, while the present limits are still not sensitive enough to test the parameter space relevant for the anomalies, with 300 fb^{-1} most of the relevant space will be covered experimentally. Also, with more and more luminosity, this channel will put *upper limits* on the LQ mass (when imposing a successful fit of the $R(D^{(*)})$ anomaly). This complements the *lower limits* usually derived from pair-production searches.

The $c\bar{c} \to N_R \bar{N}_R$ channel gives rise to a fully invisible final state. In this case one can ask for the presence of an initial state radiation jet onto which one can trigger, thus obtaining a mono-jet signature. The CMS collaboration has performed this analysis for the case of a coloured scalar mediator connecting the SM visible sector with a dark matter candidate [99]. By assuming only couplings with the up type quarks, and fixing this coupling to one, they obtain a bound of 1350 GeV on the LQ mass. This corresponds to a parton level cross-section of ~ 16 fb for $p_T^j > 250$ GeV, which we use as an upper limit on the monojet cross-section to set the limits on the vector LQ mass and couplings. For the $b\bar{b} \to \tau\tau$ process, we impose the bound obtained in [100] and rescale it with the $\sqrt{\mathcal{L}}$ factor in order to get the estimate for the projected sensitivity.

The current and projected constraints arising from the off-shell analyses are shown together with those from LQ pair production searches in figure 2. We observe that monojet

JHEP10(2018)092

and $\tau\tau$ searches nicely complement direct searches for small and large $g^d_{b\tau}$, respectively. Impressively, the off-shell search for τN_R, which exclude the region on the *right* of the contours, will completely close the parameter space already with $300\,\text{fb}^{-1}$ of integrated luminosity, thus making this scenario falsifiable in the near future.

3.2 Scalar LQ S_1

Pair-production. As for the vector case, also the interactions of the scalar LQ in eq. (2.11) can be constrained in several ways. The on-shell production of a pair of scalar LQs is the dominant search channel at the LHC, which only depends on the LQ mass and branching ratios.[6] Since in section 2 we showed that the couplings $\lambda^q_{s\mu}$ and $\lambda^q_{b\mu}$ of S_1 that are needed to fit $R(K^{(*)})$ might be incompatible (depending on the SM prediction considered) with the constraints arising from $B_s - \bar{B}_s$ mixing, we set them to zero for the forthcoming discussion. For LQ pair production searches the phenomenology of the scalar LQ is thus determined by the following ratio

$$\frac{\Gamma(S_1 \to \bar{b}\bar{N}_R)}{\Gamma(S_1 \to \bar{c}\bar{\tau})} \sim \frac{|\lambda^d_{bN}|^2}{|\lambda^u_{c\tau}|^2}. \tag{3.3}$$

The CMS analysis [97] searches LQs decaying into the $b\bar{b}\nu\bar{\nu}$ final state. This analysis can be directly applied to the case of the scalar LQ, given than the only difference with the decay mode targeted by the experimental analysis is the nature of the final state neutrino, which however does not strongly affect the kinematics of the event. For the $2c2\tau$ final state no direct searches exist. The CMS analysis in [94], recently updated in [95], targets the $b\bar{b}\tau^+\tau^-$ decay mode and in principle cannot be applied to our scenario. We however observe that, for 100% branching ratios, the cross section in the analysis signal region (σ_{SR}) for the LQ $\to c\tau$ or $b\tau$ cases is given by

$$\begin{aligned} \sigma^{\text{LQ}\to c\tau}_{\text{SR}} &= \sigma^{\text{LQ}}_{\text{Th.}} \times [\mathcal{A}\times\epsilon]_{LQ\to c\tau} \times (2\epsilon_c(1-\epsilon_c)+\epsilon_c^2) \\ \sigma^{\text{LQ}\to b\tau}_{\text{SR}} &= \sigma^{\text{LQ}}_{\text{Th.}} \times [\mathcal{A}\times\epsilon]_{\text{LQ}\to b\tau} \times (2\epsilon_b(1-\epsilon_b)+\epsilon_b^2) \end{aligned} \tag{3.4}$$

where ϵ_c is the probability to mis-identify a c-jet as a b-jet, ϵ_b is the b-jet tagging efficiency, $[\mathcal{A}\times\epsilon]_i$ is the acceptance for the considered final state and $\sigma^{\text{LQ}}_{\text{Th.}}$ is the LQs pair production cross section. Since the kinematics of the event is not expected to change if a final state quark is a b-jet or a c-jet, the ratio of the number of events in the signal region for the case of the $b\tau$ and $c\tau$ final state is simply given by[7]

$$\frac{\sigma^{\text{LQ}\to c\tau}_{\text{SR}}}{\sigma^{\text{LQ}\to b\tau}_{\text{SR}}} = \frac{2\epsilon_c(1-\epsilon_c)+\epsilon_c^2}{2\epsilon_b(1-\epsilon_b)+\epsilon_b^2}, \tag{3.5}$$

i.e. the cross section is rescaled by a factor only dictated by the jet tagging efficiencies. In particular the upper limit on the cross section has to be divided by the factor in eq. (3.5)

[6] To compute the LQ pair production rates we have used next-to-leading-order QCD cross section for squarks pair production from the LHC Higgs Cross Section Working Group https://twiki.cern.ch/twiki/bin/view/LHCPhysics/SUSYCrossSections.

[7] The analysis requires only one b-tag jet, while no flavour requirement is imposed on the second jet.

JHEP10(2018)092

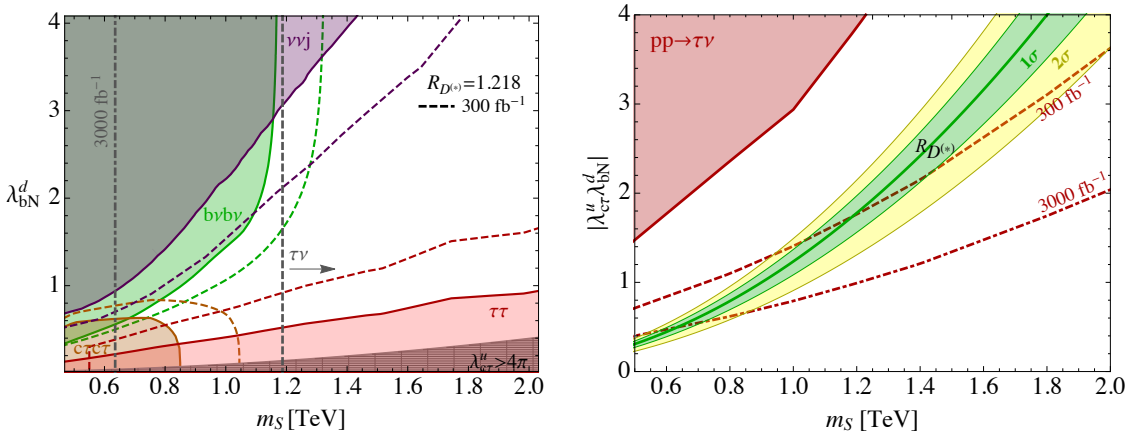

Figure 4. (Left) Limits arising from direct and indirect LHC searches in the $m_S - \lambda^d_{bN}$ plane, with $\lambda^u_{c\tau}$ fixed to fit the central value of $R_{D^{(*)}}$. Current limits are shown as shaded areas, while projections for 300 fb^{-1} of integrated luminosity as dashed lines. The arrow indicates the region excluded by the $\tau\nu$ search. The region where $\lambda^u_{c\tau}$ becomes non perturbative is also illustrated. (Right) Limits from $\tau\nu$ searches in the $m_S - |\lambda^u_{c\tau}\lambda^d_{bN}|$ plane. Also shown are the 68% and 95% CL intervals around the central values of $R_{D^{(*)}}$, eq. (1.2).

which is smaller than 1. For concreteness we use the 70% b-tag efficiency working point of [94] from which we obtain $\epsilon_c \sim 20\%$ [101]. The bounds arising from LQs pair production searches are shown as green and orange shaded areas in figure 4 (left) in the $m_S - \lambda^d_{bN}$ plane for the $2b2N_R$ and $2c2\tau$ final state respectively, where $\lambda^u_{c\tau}$ has been fixed to match the central value of $R(D^{(*)})$, see eq. (2.14). We also again show the projections for a higher LHC integrated luminosity, namely 300 fb^{-1}. All together we see that current direct searches are able to constrain scalar LQs with a mass of $\sim$ 1 TeV when the dominant coupling is the one to bN while a weak constraints of $\sim$ 600 GeV can be set if the dominant coupling is the one to $c\tau$, with these limits becoming $\sim$ 1.3 TeV and 1 TeV respectively for 300 fb^{-1}.

Off-shell exchange. Similarly to the vector LQ, also the scalar S_1 can be exchanged in t-channel in $c\bar{b} \to \tau\bar{N}_R$, $b\bar{b} \to N_R\bar{N}_R$, and $c\bar{c} \to \tau\tau$ processes. Also in this case the $c\bar{b} \to \tau\bar{N}_R$ process directly tests the same couplings involved in the explanation of the $R(D^{(*)})$ anomalies. The experimental limits, and future projections, are obtained from the ATLAS analysis [98] in the same way as described for the vector LQ case. The derived limits in the $m_S - |\lambda^d_{bN}\lambda^u_{c\tau}|$ plane, superimposed with the 68% and 95% CL intervals around the central values for $R(D^*)$, are shown in the right panel of figure 4. Also in the scalar LQ case this search will put an *upper limit* on the LQ mass m_S once the fit of the charged current flavour anomalies is imposed, and the high luminosity phase of the LHC with 3000 fb^{-1} of integrated luminosity will cover the whole relevant parameter space.

The $b\bar{b} \to N_R\bar{N}_R$ final state can be constrained by monojet searches in an analogous way as done for the vector LQ. The excluded parameter space is shown as a purple region in the left panel of figure 4.

The limits on the $c\bar{c} \to \tau\tau$ process can be obtained from the ones computed in [100] for $b\bar{b} \to \tau\tau$ case (shown in the bottom panel of figure 6 of [100]) by taking into account

JHEP10(2018)092

the different parton luminosities for the two different initial state quarks. In particular, we approximate the $R_{cb}(\hat{s}) = \mathcal{L}_{cc}(\hat{s})/\mathcal{L}_{bb}(\hat{s}) \approx 2.5$ ratio as constant and rescale the limit on the $y_L^{b\tau}$ coupling in [100] neglecting the interference of the signal with the SM background: $\text{limit}(|\lambda^u_{c\tau}|) \approx \text{limit}(|y_L^{b\tau}|)R_{cb}^{1/4}$. The resulting excluded region is shown as a red region in the left panel of figure 4.

All together the current and projected constraints arising from these three analyses are shown together with the one arising from LQ pair production searches in the left panel of figure 4. We observe that $\tau\tau$ searches nicely complement direct searches for small λ^q_{bN} while also in this case searches for τN_R, which again exclude the region on the right of the contours, will almost completely close the parameter space already with $300\,\text{fb}^{-1}$ of integrated luminosity.

4 Neutrino masses and decays

The phenomenology of both the SM-like and sterile neutrino crucially depends on whether only the $R(D^{(*)})$ anomalies are addressed or if also the neutral-current ones are. This is particularly relevant for the vector LQ, since this state allows to explain both without any tension with flavour, precision, or collider constraints. For this reason in the following we discuss both scenarios separately, stressing the main consequences for each of them.

4.1 Addressing only $R(D^{(*)})$

The operator responsible for reproducing the $R(D^{(*)})$ anomalies, eq. (1.1), generates a Dirac mass term $\mathcal{L} \sim m^D \bar{\nu}_L^\tau N_R + h.c.$ at two loops, where one can estimate [42, 43]

$$m^D_{R(D^{(*)})} \sim \frac{g^2}{2(16\pi^2)^2} \frac{c_{R_D} m_b m_c m_\tau V_{cb}}{\Lambda^2} \sim 10^{-3}\ \text{eV}\ . \tag{4.1}$$

Such a small contribution to neutrino masses does not affect their phenomenology in a relevant way and therefore can be mostly neglected. In this scenario the leading decay mode for the heavy neutrino is $N_R \to \nu_\tau \gamma$, which also arises at two loops from the same operator, with a rate (see ref. [43] and references therein)

$$\tau_{N_R \to \nu_\tau \gamma} \sim 10^{25} \left(\frac{\text{keV}}{m_{N_R}}\right)^3 s\,, \tag{4.2}$$

which is much larger than the age of the Universe.

4.2 Addressing also $R(K^{(*)})$

If one wants to address also the neutral-current anomalies $R(K^{(*)})$ the situation becomes more complicated. In the following we focus on the model with the vector LQ, since it is the one which allows to do so without introducing tension with other observables. The chirality-flipping operators O_{lNuq} induce a Dirac mass term between N_R and ν_μ at one loop, see figure 5, and with less suppression from light fermion masses:

$$m^D_{(R(D^{(*)})+R(K^{(*)}))_U} \sim \frac{1}{16\pi^2} g^u_{cN} m_c \left(g^q_{b\mu} V_{cb} + g^q_{s\mu} V_{cs}\right) \sim 10\ \text{keV}\,, \tag{4.3}$$

where we used the constraint in eq. (2.7) and assumed $g^q_{s\mu} \sim V_{cb} g^q_{b\mu}$.

JHEP10(2018)092

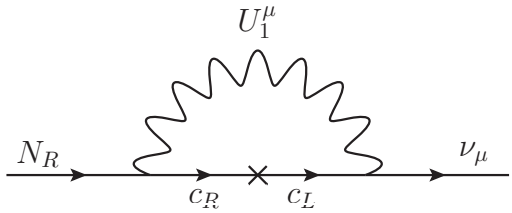

Figure 5. Diagram responsible for generating a $\nu - N_R$ Dirac mass term at one loop in the vector LQ model in case both charged- and neutral-current anomalies are addressed.

Such large neutrino masses are of course incompatible with experiments. One possible solution is to finely tune these radiative contributions with the corresponding bare Dirac neutrino mass parameter, in order to get small masses. A more natural and elegant solution can instead be found by applying the inverse see-saw mechanism [48, 49] (see also [50]). This was also employed recently in the context of the B-meson anomalies in ref. [58]. In its simplest realisation, this mechanism consists in adding another sterile state[8] $\tilde{S}_L$ with a small Majorana mass μ_S and Dirac mass M_R with $\tilde{N}_R$. By defining $n = (\tilde{\nu}_L, \tilde{N}_R^c, \tilde{S}_L)^t$ the mass Lagrangian $\mathcal{L}_n = -1/2\, \bar{n}\, M_n\, n^c$ can be written in terms of the following mass matrix

$$M_n = \begin{pmatrix} 0 & m^D & 0 \\ m^D & 0 & M_R \\ 0 & M_R & \mu_S \end{pmatrix} , \tag{4.4}$$

Diagonalising the matrix, in the limit $\mu_S \ll m^D < M_R$, the spectrum presents a light SM-like Majorana neutrino with mass

$$m_{\nu_L}^{\text{light}} \sim \left(\frac{m^D}{\sqrt{(m^D)^2 + M_R^2}} \right)^2 \mu_S \tag{4.5}$$

and two heavy psuedo-Dirac neutrinos $N_{R_{1,2}}$ with masses $m_{N_R} \sim \sqrt{(m^D)^2 + M_R^2}$ and a splitting of order μ_S. A small enough μ_S can therefore control the smallness of the contribution to the light neutrinos without the need of any fine tuning. The mixing angle between the light neutrinos and the sterile one is given by

$$\theta_{\nu_\mu N} \sim \frac{m^D}{M_R} \lesssim 10^{-2} , \tag{4.6}$$

where we used the (conservative) experimental bound of ref. [102] for sterile neutrinos with masses $m_{N_R} \sim 10$ MeV. Indeed, this limits puts a lower bound on the mass of the sterile neutrinos $m_{N_R} \gtrsim 10^2 m^D \sim 1$ MeV which is relevant for the cosmological analysis of the model.

[8] In this subsection we use the tilde to denote gauge eigenstates, and reserve the notation without the tilde for the mass eigenstates.

JHEP10(2018)092

In this case, the main decay modes of the sterile neutrino are $N_R \to 3\nu, \nu_\mu e^+ e^-$ via the mixing with ν_μ and an off-shell Z boson exchange [43]:

$$\begin{aligned} \tau_{N_R \to 3\nu} &\approx \left(\frac{G_f^2}{144\pi^3} \left(3|g^Z_{\nu_L}|^2 + |g^Z_{e_L}|^2 + |g^Z_{e_R}|^2\right) \theta^2_{\nu_\mu N} m^5_{N_R} \right)^{-1} \\ &\sim 2.5 \times 10^5 \left(\frac{10 \text{ MeV}}{m_{N_R}}\right)^5 \left(\frac{10^{-6}}{\theta^2_{\nu_\mu N}}\right) \; s \; . \end{aligned} \tag{4.7}$$

In this scenario N_R decouples from the SM thermal bath at a temperature of $\sim 300\,\text{MeV}$ (see next section), then becomes non relativistic and behaves like matter, comes to dominate the energy density after big bang nucleosynthesis (BBN), and decays into neutrinos and electrons before the epoch of matter radiation equality. This would generate a large contribution to the SM neutrino and electron energy densities before CMB, which is not cosmologically viable.

To avoid this problem N_R should decay before BBN, which requires $\tau_{N_R} < 1s$. Looking at the leading decay mode, eq. (4.7), a simple way to achieve this is to increase both $m_{N_R} \approx M_R$ and m_D such that $m_{N_R} \gtrsim 130$ MeV and $\theta_{\nu_\mu N} \sim 10^{-3}$ (satisfying the limits from ref. [102]). In this case a suitable short lifetime can be obtained. Such a mass of the sterile neutrino is close to the bound where it could potentially have an effect on the kinematics of $B \to D^{(*)}\tau\nu$. However a precise analysis of this scenario can only be performed with all details of the experimental analysis available. Interestingly, there are almost no constraints on $\theta_{\nu_\mu N}$ in the window of $\sim 30-40\,\text{MeV}$ (roughly the mass difference between the charged pion and the muon, see for example [103]). This window provides an opportunity for a short enough lifetime of N_R in this model. Future measurements by DUNE [104] and NA62 [103] will be able to test the scenarios with $m_{N_R} \gtrsim 130\,\text{MeV}$ and with $m_{N_R} \in [30, 40]\,\text{MeV}$.

Another possibility is to add a mixing of N_R with the τ neutrino, by adding a suitable Dirac mass term. In this case the lower limits on $\theta_{\nu_\tau N}$ [102] are much weaker, allowing $\theta^2_{\nu_\tau N} \lesssim 10^{-3}$ for $m_{N_R} \approx 100$ MeV and even larger ones for lighter masses. This allows to reduce even further the N_R lifetime, while keeping the N_R mass below the 100 MeV threshold.

5 Cosmology of N_R

In this section we discuss cosmological bounds and opportunities in the presence of right handed neutrinos. As we saw in the previous section, if we only want to address the $R(D^{(*)})$ anomaly the right handed neutrino can be as light as 10^{-3} eV and is cosmologically stable. Instead, if we also address the $R(K^{(*)})$ anomaly then it is much heavier and with a shorter lifetime. In particular we showed that it must decay before BBN in order to be a viable option. In this section we focus on the case where only $R(D^{(*)})$ is addressed and N_R is cosmologically stable.

5.1 Relic density

Addressing only $R(D^{(*)})$, N_R can be light and has a lifetime longer than the age of the universe. It therefore contributes to the DM relic density. Fitting the $R(D^{(*)})$ anomaly

JHEP10(2018)092

fixes the strength of the interaction of N_R with the right handed b, c, τ. This in turn implies that N_R was in thermal equilibrium in the early universe, and determines when it decoupled from the thermal bath. Solving the Boltzmann equation (see appendix A) we find that N_R freezes out at a temperature of $\sim 300\,\text{MeV}$, slightly above the QCD phase transition. Since $m_{N_R} \lesssim 100\,\text{MeV}$ in order to explain $R(D^{(*)})$, it is relativistic at freeze-out. Its relic abundance today, assuming a lifetime longer than the age of the universe, is then [105, 106]

$$\begin{aligned}\Omega_N h^2 &= \frac{s_0 m_{N_R}}{\rho_c}\left[\left(\frac{n}{s}\right)_{\text{today}} = \left(\frac{n}{s}\right)_{\text{decoupling}}\right] \\ &= \frac{s_0 m_{N_R}}{\rho_c}\left[\frac{\frac{3}{4\pi^2}\times 2\times\zeta(3)T_{\text{dec}}^3}{\frac{2\pi^2}{45}T_{\text{dec}}^3 g_{*S}(T_{\text{dec}})}\right] = 0.12\,\frac{50}{g_{*S}(T_{\text{dec}})}\,\frac{m_{N_R}}{50\text{ eV}}\,. \end{aligned} \tag{5.1}$$

Here $s_0 = 2891\text{ cm}^{-3}$ is the present entropy density and $\rho_c = 1.05\times 10^4\ h^2\,\text{eV cm}^{-3}$ the critical energy density [71]. We find a yield $\left(\frac{n}{s}\right)_{\text{today}}$ which ranges between 8.3×10^{-3} and 1.3×10^{-2}, and correspondingly[9] $g_{*S}(T_{\text{dec}})$ in the range between 35 and 60. For the sake of the estimates which follow, we take $g_{*S}(T_{\text{dec}}) = 50$ as our reference value. We see that $m_{N_R} \approx 50$ eV can account for the required amount of DM in the universe. However this is now a hot relic, and as such it is not consistent with structure formation. To make it comply with these bounds, we can simply lower its mass. For $m_{N_R} \lesssim$eV, the right handed neutrino makes up less than 2% of the DM abundance and it is safely within the structure formation bound [107].

5.2 ΔN_{eff}

Such a light N_R contributes to the number of effective relativistic species, N_{eff}. The quantity ΔN_{eff} is defined as the ratio of the energy density in dark radiation and that in one species of SM neutrino at the time of BBN,

$$\Delta N_{\text{eff}} = \frac{3\rho_{dr}(t_{BBN})}{\rho_\nu(t_{BBN})} = \left(\frac{T_{N,\text{BBN}}}{T_{\nu,\text{BBN}}}\right)^4. \tag{5.2}$$

The ratio of the temperatures can be found using the total entropy conservation in the visible sector, just after the right-handed neutrino decoupled from the thermal bath [108]:

$$\frac{T_{N,\text{BBN}}}{T_{\nu,\text{BBN}}} = \left(\frac{g_{*S}(T_{\text{BBN}})}{g_{*S}(T_{\text{dec}})}\right)^{1/3}. \tag{5.3}$$

Thus, from eq. (5.2), we get

$$\Delta N_{\text{eff}} = \left(\frac{10.73}{g_{*S}(T_{\text{dec}})}\right)^{4/3} \sim 0.13\left(\frac{50}{g_{*S}(T_{\text{dec}})}\right)^{4/3}, \tag{5.4}$$

which is within the experimental constraints [109].

[9] The final yield depends on whether the UV completion of the model allows, on top of $bc \leftrightarrow N_R\tau$, also one of the $N_R N_R \leftrightarrow bb, \tau\tau, cc$ scattering processes. In the latter case the freeze-out of N_R is slightly delayed and the yield turns out to be slightly higher, see appendix A. The value of $g_{*S}(T)$ has a strong dependence on T when we are close to the QCD phase transition, as in this case. We use $g_{*S}(T_{\text{dec}}) = 50$ in the estimates that follow. The reader should keep in mind that, while in the right ballpark, this number has some degree of uncertainty.

JHEP10(2018)092

We then conclude that a minimal model with a single right-handed neutrino N_R lighter than an eV can explain the $R(D^{(*)})$ anomalies and evade all the relevant cosmological constraints. However N_R can only be a small fraction of the DM in this case.

5.3 The dark matter option and entropy injection

We have shown that in the minimal scenario N_R is a hot relic and can only constitute a small fraction of the observed DM energy density. It is interesting to explore the possibility of raising the N_R mass to the keV range to make it a warm dark matter candidate. From eq. (5.1) we see that $m_{N_R} \sim$ keV results in overclosure of the universe. We can then consider adding to the model a second heavier right-handed neutrino, χ_R, whose decay produces enough entropy to dilute the abundance of N_R [110, 111].[10] The dilution factor, defined as

$$D \equiv \frac{S_{\text{after } \chi \text{ decay}}}{S_{\text{before } \chi \text{ decay}}}\,, \tag{5.5}$$

modifies the relic density and ΔN_{eff} as

$$\begin{aligned} \Omega_N h^2 &= \frac{1}{D} 0.12 \frac{50}{g_{*S}(T_{\text{dec}})} \frac{m_{N_R}}{50 \text{ eV}}\,, \\ \Delta N_{\text{eff}} &= \frac{1}{D^{4/3}} \left(\frac{10.73}{g_{*S}(T_{\text{dec}})} \right)^{4/3}. \end{aligned} \tag{5.6}$$

Note that we need D of order 20 if we want to push m_{N_R} to the keV range. In what follows we study if we can achieve such a dilution in a rather minimal setup.

We assume that the heavier right-handed neutrino χ_R, analogously to N_R, is subject to the interaction

$$\mathcal{L}_{\chi_R} = \frac{\lambda}{\Lambda_\chi^2} (\bar{c}_R \gamma_\mu b_R)(\bar{\tau}_R \gamma^\mu \chi_R)\,. \tag{5.7}$$

We want χ_R to decouple from the thermal bath at high temperature (but still below Λ_χ, so the use of the effective interaction is justified), to come to dominate the energy density of the universe, then to decay and reheat the universe between 300 MeV (the decoupling temperature of N_R) and BBN. We discuss each step in turn.

χ_R decouples from the thermal bath when $\Gamma = n\langle\sigma v\rangle \simeq H$, with $\sigma = \frac{\lambda^2 s}{16\pi\Lambda_\chi^4}$ (here s is the centre of mass energy squared). Assuming χ_R is relativistic at decoupling, we find

$$T_\chi = 3 \times 10^{-2} g_*^{1/6} \lambda^{-2/3} \text{ GeV}\,, \tag{5.8}$$

and a yield

$$Y_\chi = \frac{n_\chi}{s} = \frac{45}{\pi^4 g_{*S}(T_{\chi,\text{decoupling}})}\,. \tag{5.9}$$

Then, as the universe expands and the temperature decreases, χ_R becomes non relativistic, and eventually dominates the energy density. It decays when $\Gamma_\chi \simeq H_\chi$, with the Hubble parameter

$$H_\chi^2 = \frac{\rho_\chi}{3M_p^2} = \frac{M_\chi s(T_{\text{before } \chi \text{ decay}}) Y_\chi}{3M_p^2}\,, \tag{5.10}$$

[10] For a recent application of the entropy dilution in the models with right-handed neutrinos see [112–114].

JHEP10(2018)092

and the decay rate into b, c, τ

$$\Gamma_\chi \simeq \frac{1}{1536\,\pi^3}\,\frac{\lambda^2}{\mathrm{TeV}^4}\,M_\chi^5\,. \tag{5.11}$$

We find the reheat temperature, $T_{\text{after }\chi\text{ decay}}$, assuming that the energy density of χ_R is instantaneously converted into radiation at decay,

$$\frac{\pi^2}{30} g_* T^4_{\text{after }\chi\text{ decay}} = \rho_\chi \simeq 3\Gamma_\chi^2 M_p^2\,. \tag{5.12}$$

This temperature must be above BBN, but below the N_R decoupling temperature:

$$1\text{ MeV} < T_{\text{after }\chi\text{ decay}} < 300\text{ MeV}\,. \tag{5.13}$$

The dilution factor can be expressed as [110, 111]

$$D = \frac{g_*(T_{\text{after }\chi\text{ decay}})T^3_{\text{after }\chi\text{ decay}}}{g_*(T_{\text{before }\chi\text{ decay}})T^3_{\text{before }\chi\text{ decay}}} \simeq 1.8\langle g_*^{1/3}\rangle^{3/4}\frac{M_\chi Y_\chi}{\sqrt{M_p\Gamma_\chi}} = 1.8\frac{M_\chi Y_\chi}{T_{\text{after }\chi\text{ decay}}}\,. \tag{5.14}$$

D is shown in figure 6 in the M_χ vs. λ plane as black contours, where we see that the entropy injection factor can reach at most ~ 100. It is instructive to trade the parameters M_χ and λ for T_χ and $T_{\text{after }\chi\text{ decay}}$, using eqs. (5.12), (5.8), (5.11). Then the expression for the D becomes

$$D = \frac{1.8 M_\chi Y_\chi}{T_{\text{after }\chi\text{ decay}}} \simeq 0.02\left(\frac{T_\chi}{T_{\text{after }\chi\text{ decay}}}\right)^{\frac{3}{5}}\left(\frac{\Lambda_\chi}{\mathrm{TeV}}\right)^{4/5}, \tag{5.15}$$

which indicates that the maximal value can be achieved for the maximal decoupling temperature T_χ and the minimal reheat temperature. As in our scenario we restrict to a decoupling temperature below the mediator mass, ~ 1 TeV, the maximal entropy dilution that can be achieved is $D_{\max} \sim 100$. If we consider a higher decoupling temperatur, the dilution factor does not improve. The reason is that above the mediator mass the cross section for the $bc \leftrightarrow \tau\chi$ scattering process scales as $1/s$, rather than s/Λ_χ^4. As a result the reaction rate $n\langle\sigma v\rangle$ is linear in T, implying that the process is out of equilibrium at very high temperatures, and freezes in at lower temperatures. When the temperature drops below Λ_χ we are back to the scenario we have studied above.

We are now in the position to assess whether such a dilution factor leads to a successful model. We see from eq. (5.6) that we can raise m_{N_R} up to 5 keV and have N_R contribute to the totality of dark matter energy density. However, for this mass the decay $N_R \to \nu\gamma$ is too fast (see eq. (4.2)) and excluded by X-ray measurements, which put a bound $\tau_{N_R\to\nu\gamma} > 10^{26-27}$ s in that region [115, 116]. To avoid this bound, we should push m_{N_R} down to ~ 1 keV. This is in some tension with constraints on warm dark matter from the Lyman-α forest (see for example [116]), which prefers a sterile neutrino heavier than 3–5 keV. However, due to the large entropy dilution, our N_R is slightly colder and likely to comply with the Lyman-α bound also when $m_{N_R} \sim 1$ keV. Further detailed studied are needed to confirm if this is the case.

JHEP10(2018)092

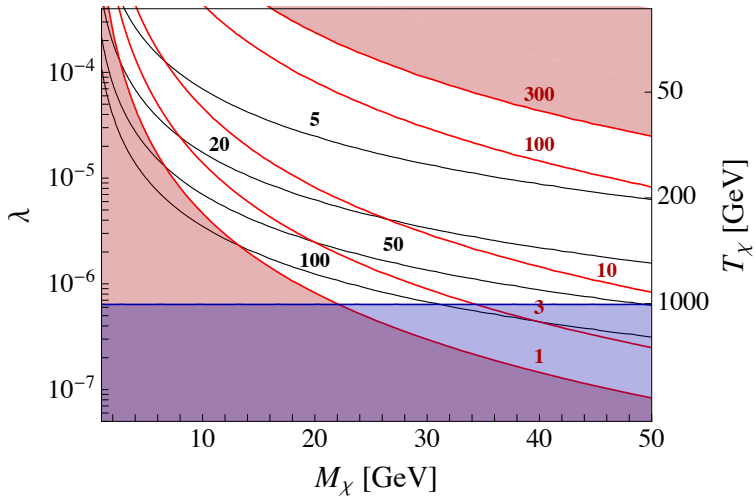

Figure 6. Isocontours of the entropy injection D (black lines). The lower red area is excluded because the reheated temperature $T_{\text{after } \chi \text{ decay}}$ is below 1 MeV and the upper red area becase the reheated temperature is above right handed neutrino decoupling temperature. Red contours indicate $T_{\text{after } \chi \text{ decay}}$ in MeV. T_χ, shown in the right axis, is the decoupling temperature of χ_R from the interaction in eq. (5.7).

6 Conclusions

The set of deviations from the Standard Model observed in various B-meson decays, from different experiments and in various different observables, is one of the most compelling experimental hints for BSM physics at the TeV scale ever obtained. Even more interesting is the possibility that all the observed deviations could be explained in a coherent manner by the same new physics. This has been the focus of a large effort from the theory community in recent years and several attempts have been put forward to achieve this goal. It became clear that this is not an easy task, in particular due to the fact that the large size of the required new physics effect to fit the $R(D^{(*)})$ anomalies generates tensions with either high-p_T searches or other flavour observables. In this spirit, it has become important to look for other possible solutions to the anomalies with different theoretical assumptions, which might help to evade the constraints. One such possibility is that the BSM operator contributing to $R(D^{(*)})$ does not involve a SM neutrino but a sterile right-handed neutrino N_R. If the operator has a suitable right-right vector structure and the sterile neutrino is light enough, the the kinematics of the process remain SM-like and the solution is viable.

In this paper we study two possible tree-level mediators for such operator in a simplified model approach: the vector leptoquark U_1^μ and the scalar leptoquark S_1. In the first part of the paper we explore the possibility that these mediators could generate both charged- and neutral-current B-physics anomalies. We find that the vector U_1^μ, which contributes to $b \to s\mu\mu$ at the tree-level, provides a viable fit with no tension with any other flavour observable. The scalar S_1, instead, contributes to the neutral-current process at one loop, thus requiring larger couplings to fit $R(K^{(*)})$. This generates a tension with the bound from B_s-$\bar{B}_s$ mixing which makes the combined solution of both class of anomalies from this mediator disfavoured. For both models we study the present constraints, and

JHEP10(2018)092

future projections, from direct searches at the LHC, including all relevant on-shell LQ pair-production modes as well as channels where the LQ is exchanged off-shell in the t-channel. We find that at present both scenarios are viable, but already with $300\,\text{fb}^{-1}$ of luminosity LHC will test almost all the viable parameter space. In particular, the search in the $\tau\nu$ final state, which directly test the interactions relevant for the $R(D^{(*)})$ anomalies, puts *upper limits* on the LQ mass and in the future will completely cover the region which fits the anomalies.

In the second part of the paper we study the phenomenology of the sterile neutrino N_R. This depends crucially on whether or not both classes of anomalies are addressed or only the charged-current ones are. In the former case a Dirac mass term with the muon neutrino is generated at one loop with a size of tens of keV. In order to keep the SM neutrinos light it is possible to employ the inverse see-saw mechanism, by introducing another sterile neutrino with a small Majorana mass and a large Dirac mass with N_R. The outcome of this is that the SM-neutrinos are light but the sterile ones are above 10 MeV. The mixing between the muon and sterile neutrino induces a fast decay of N_R, rendering it unstable cosmologically. To avoid issues with the thermal history of the Universe it should decay before BBN, which requires its mass to be ~ 100 MeV.

If instead only the $R(D^{(*)})$ anomalies are addressed the picture changes completely. In this case a Dirac mass term with the tau neutrino is generated at two loops and it is small enough to not have any impact in neutrino phenomenology. The main decay of N_R in this case is into $\nu_\tau\gamma$ and arises at two loops as well, with a lifetime much longer than the age of the Universe. In order not to overclose the Universe energy density its mass should be below ~ 50 eV, which makes it a hot relic. The constraints on the allowed amount of hot dark matter impose an upper limit on its contribution to the present dark matter density, which translates into an upper bound for the mass $m_{N_R} \lesssim$ eV. If the sterile neutrino is to constitute the whole dark matter, an entropy injection at late times is necessary in order to dilute its abundance. This can be obtained, for example, by adding another heavy sterile neutrino which decays into SM particles after N_R decouples. In this case we find that N_R could be a warm dark matter candidate with a mass $\sim$ (few keV). This option is highly constrained by current cosmological and astrophysical observations. While our model seems to have a small region of viable parameter space, a conclusive statement requires further detailed studies.

To conclude, the U_1^μ model presented in this paper allows to fit both charged- and neutral-current anomalies with no tension at all with present low- and high-p_T bounds. The sterile neutrino in this case is cosmologically unstable, decaying before BBN happens. In case one aims at only solving the $R(D^{(*)})$ anomalies, instead, the neutrino is stable and if it is light enough it satisfies all cosmological constraints. With some additions to the model, in particular a mechanism for entropy injection after it decouples, it can also be a candidate for dark matter at the keV scale.

Acknowledgments

We thank Marco Nardecchia for discussions and for collaborating in the early stages of the work. We also thank Andrea Romanino and Serguey Petcov for useful discussions.

JHEP10(2018)092

A Boltzmann equation

To find the freeze-out temperature of the light right-handed neutrino N_R, we solve the Boltzmann equation

$$s_e(z)zH(z)\left(1-\frac{z}{3g_{*S}(z)}\frac{dg_{*S}}{dz}\right)^{-1}\frac{dY_N}{dz} = \left(-\frac{Y_N}{Y_N^{eq}}+1\right)\left(\gamma(Nb\to\tau c)+\gamma(Nc\to\tau b)+\gamma(N\tau\to bc)\right) . \tag{A.1}$$

Here we consider only the effective interaction needed to explain the $R(D^{(*)})$ anomaly, which implies that in the 2 to 2 scattering processes in the thermal bath there is only one N_R involved. We use the following conventions, inspired by ref. [117],

$$z\equiv\frac{m_b}{T}\,,\qquad Y_i=\frac{n_i}{s_e}\,,\qquad n_{i,\mathrm{rel}}^{eq}=\frac{g_iT^3}{\pi^2}\,,\qquad s_e=\frac{g_{*S}2\pi^2}{45}T^3\,, \tag{A.2}$$

$$H=\frac{1}{2t}=\frac{1.66\sqrt{g_*}m_b^2}{z^2m_{\mathrm{pl}}}\,, \tag{A.3}$$

$$\gamma(ij\to mn)=\frac{g_ig_jm_b^6}{32\pi^4z}\int_{x_{\min}}^{\infty}dx\;x\sqrt{x}\;K_1(z\sqrt{x})\;\lambda\left(1,\frac{m_i^2}{xm_b^2},\frac{m_j^2}{xm_b^2}\right)\sigma(xm_b^2)\,, \tag{A.4}$$

$$x_{\min}=\mathrm{Max}\left[\frac{(m_i+m_j)^2}{m_b^2},\frac{(m_m+m_n)^2}{m_b^2}\right]\,, \tag{A.5}$$

$$\lambda(a,b,c)=(a-b-c)^2-4bc\,, \tag{A.6}$$

where we are using the Maxwell-Boltzmann statistics for simplicity. Here g_i is the number of internal degrees of freedom of the particle (2 for a Weyl fermion), K_1 is a Bessel function, and

$$x\equiv\frac{s}{m_b^2}\,,\qquad \sigma(xm_b^2)=\frac{xm_b^2}{16\pi(\Lambda/\sqrt{c_{R_D}})^4}=\frac{s}{16\pi(\Lambda/\sqrt{c_{R_D}})^4}\,, \tag{A.7}$$

with s the centre of mass energy squared.

Depending on the mediator in the UV completion, one will also have effective operators which introduce either the $N_RN_R\leftrightarrow cc, N_RN_R\leftrightarrow bb, N_RN_R\leftrightarrow\tau\tau$ scattering processes. Particularly important is the $N_RN_R\leftrightarrow cc$ since charm is lighter than τ and b quark and is less Boltzmann suppressed, keeping N_R in thermal equilibrium for a little longer. As a result, the effect of including the $N_RN_R\leftrightarrow cc$ process is to slightly delay the freeze-out of N_R. To take it into account we can add the term

$$\left(-\frac{Y_N^2}{(Y_N^{eq})^2}+1\right)\gamma(NN\to cc) \tag{A.8}$$

to the right hand side of eq. (A.1). We show in figure 7 how Y_N evolves as a function of z. We fix the interaction strength to $\Lambda/\sqrt{c_{R_D}}=1.27\,\mathrm{TeV}$, which is the value which fits the $R(D^{(*)})$ anomaly, see eq. (1.3). When the only processes are those in eq. (A.1), we find the freeze-out temperature

$$T_{\mathrm{FO},N}\simeq 350\ \mathrm{MeV}\,, \tag{A.9}$$

JHEP10(2018)092

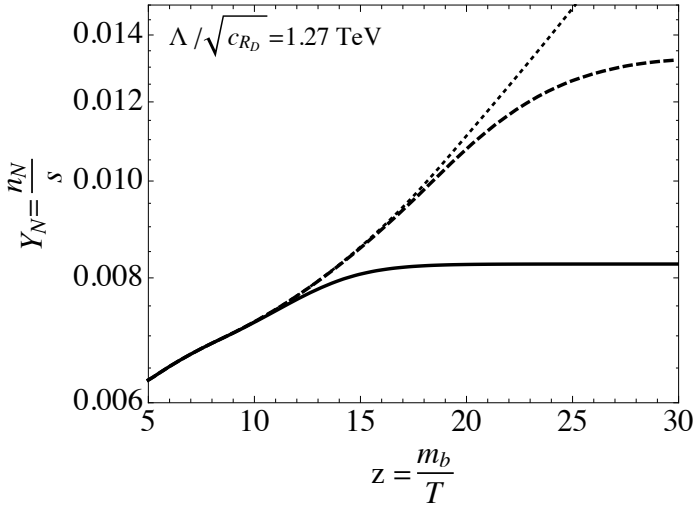

Figure 7. The dotted line shows the equilibrium distribution Y_N^{eq}, the solid line is for Y_N which solves the Boltzmann equation (A.1), while the dashed line includes also the contribution from eq. (A.8). We see that freeze-out occurs at $z_{\mathrm{FO},N} \simeq 12$ (solid line) for processes involving only one N_R, at $z_{\mathrm{FO},NN} \simeq 17$ (dashed line) when we also include the process $N_R N_R \leftrightarrow cc$ [see eq. (A.8)].

the final yield

$$Y_{N,0} = 8.3 \times 10^{-3}\,, \tag{A.10}$$

and

$$g_{*S} = \frac{45}{\pi^4 Y_{N,0}} = 56\,. \tag{A.11}$$

When we include also the processes of eq. (A.8) we find

$$T_{\mathrm{FO},NN} \simeq 250 \text{ MeV}\,, \tag{A.12}$$

$$Y_{N,0} = 1.3 \times 10^{-2}\,, \tag{A.13}$$

$$g_{*S} = 35\,. \tag{A.14}$$

Note that these values of g_{*S} should be taken with a grain of salt, as we are close to the QCD phase transition and g_{*S} has a strong dependence on the temperature in this range. The quoted values are meant as a ballpark which we use for the estimates in this paper.

Analytic estimates. We can check analytically the numerical result obtained above. Let's consider only the process $N_R\tau \leftrightarrow bc$. The equation of Boltzmann above is easily manipulated into the familiar form

$$\dot{n}_N + 3Hn_N = (-n_N n_\tau^{eq} + n_N^{eq} n_\tau^{eq})\langle\sigma v\rangle\,, \tag{A.15}$$

with

$$\langle\sigma v\rangle \equiv \frac{\gamma(N\tau \to bc)}{n_N^{eq} n_\tau^{eq}}\,. \tag{A.16}$$

Written in terms of s (centre of mass energy squared) the rate density is

$$\gamma(N\tau \to bc) = \frac{T^2}{8\pi^4}\int_{s_{\min}}^{\infty} ds\; s\; \frac{\sqrt{s}}{T} K_1\left(\frac{\sqrt{s}}{T}\right)\; \lambda\left(1, 0, \frac{m_\tau^2}{s}\right)\sigma(s)\,, \tag{A.17}$$

JHEP10(2018)092

with

$$s_{\min} = (m_b + m_c)^2 \,. \tag{A.18}$$

We know that at $T = \sqrt{s_{\min}} \sim 5\,\text{GeV}$, for interactions not so much weaker than the weak force (that is for Λ in the TeV ballpark), N_R is in thermal equilibrium. Thus, to make analytic progress, we can take the limit $T \ll \sqrt{s}$. In this limit

$$\frac{\sqrt{s}}{T} K_1\left(\frac{\sqrt{s}}{T}\right) \xrightarrow[\sqrt{s} \gg T]{} \sqrt{\frac{\pi}{2}} \left(\frac{\sqrt{s}}{T}\right)^{1/2} e^{-\sqrt{s}/T} \,. \tag{A.19}$$

Because of the exponential suppression at large s, the main contribution to the integral in eq. (A.17) comes from $s \simeq s_{\min}$, so we get

$$\langle \sigma v \rangle \simeq \frac{1}{n_N^{eq} n_\tau^{eq}} \frac{T^2}{8\pi^4} s_{\min}^2 \sqrt{\frac{\pi}{2}} \left(\frac{\sqrt{s_{\min}}}{T}\right)^{1/2} e^{-\sqrt{s_{\min}}/T} \left(1 - \frac{m_\tau^2}{s_{\min}}\right)^2 \frac{s_{\min}}{16\pi(\Lambda/\sqrt{c_{R_D}})^4} \,. \tag{A.20}$$

With this we can estimate the rate at which N_R scatter off τ:

$$\Gamma \simeq n_\tau^{eq} \langle \sigma v \rangle \,. \tag{A.21}$$

Freeze out occurs when $\Gamma \simeq H$:

$$\frac{\pi^2}{2T^3} \frac{T^2}{8\pi^4} s_{\min}^2 \sqrt{\frac{\pi}{2}} \left(\frac{\sqrt{s_{\min}}}{T}\right)^{1/2} e^{-\sqrt{s_{\min}}/T} \left(1 - \frac{m_\tau^2}{s_{\min}}\right)^2 \frac{s_{\min}}{16\pi(\Lambda/\sqrt{c_{R_D}})^4} \simeq \frac{1.66\sqrt{g_*} T^2}{m_{\text{pl}}} \,. \tag{A.22}$$

With $s_{\min} = (m_b + m_c)^2$ and $\Lambda/\sqrt{c_{R_D}} = 1.27\,\text{TeV}$, we find

$$T_{\text{FO},N} \simeq 250 \text{ MeV} \,. \tag{A.23}$$

This is in good agreement with the 350 MeV result, which we read off from the plot of figure 7.

Open Access. This article is distributed under the terms of the Creative Commons Attribution License (CC-BY 4.0), which permits any use, distribution and reproduction in any medium, provided the original author(s) and source are credited.

References

[1] BaBar collaboration, J.P. Lees et al., *Evidence for an excess of $\bar{B} \to D^{(*)}\tau^-\bar{\nu}_\tau$ decays*, *Phys. Rev. Lett.* **109** (2012) 101802 [arXiv:1205.5442] [INSPIRE].

[2] BaBar collaboration, J.P. Lees et al., *Measurement of an Excess of $\bar{B} \to D^{(*)}\tau^-\bar{\nu}_\tau$ Decays and Implications for Charged Higgs Bosons*, *Phys. Rev.* **D 88** (2013) 072012 [arXiv:1303.0571] [INSPIRE].

[3] Belle collaboration, M. Huschle et al., *Measurement of the branching ratio of $\bar{B} \to D^{(*)}\tau^-\bar{\nu}_\tau$ relative to $\bar{B} \to D^{(*)}\ell^-\bar{\nu}_\ell$ decays with hadronic tagging at Belle*, *Phys. Rev.* **D 92** (2015) 072014 [arXiv:1507.03233] [INSPIRE].

[4] Belle collaboration, Y. Sato et al., *Measurement of the branching ratio of $\bar{B}^0 \to D^{*+}\tau^-\bar{\nu}_\tau$ relative to $\bar{B}^0 \to D^{*+}\ell^-\bar{\nu}_\ell$ decays with a semileptonic tagging method*, *Phys. Rev.* **D 94** (2016) 072007 [arXiv:1607.07923] [INSPIRE].

JHEP10(2018)092

[5] Belle collaboration, S. Hirose et al., *Measurement of the τ lepton polarization and $R(D^*)$ in the decay $\bar{B} \to D^* \tau^- \bar{\nu}_\tau$*, Phys. Rev. Lett. **118** (2017) 211801 [arXiv:1612.00529] [inSPIRE].

[6] LHCb collaboration, *Measurement of the ratio of branching fractions $\mathcal{B}(\bar{B}^0 \to D^{*+}\tau^-\bar{\nu}_\tau)/\mathcal{B}(\bar{B}^0 \to D^{*+}\mu^-\bar{\nu}_\mu)$*, Phys. Rev. Lett. **115** (2015) 111803 [*Erratum ibid.* **115** (2015) 159901] [arXiv:1506.08614] [inSPIRE].

[7] LHCb collaboration, *Measurement of the ratio of the $B^0 \to D^{*-}\tau^+\nu_\tau$ and $B^0 \to D^{*-}\mu^+\nu_\mu$ branching fractions using three-prong τ-lepton decays*, Phys. Rev. Lett. **120** (2018) 171802 [arXiv:1708.08856] [inSPIRE].

[8] LHCb collaboration, *Test of lepton flavor universality by the measurement of the $B^0 \to D^{*-}\tau^+\nu_\tau$ branching fraction using three-prong τ decays*, Phys. Rev. **D 97** (2018) 072013 [arXiv:1711.02505] [inSPIRE].

[9] HFLAV collaboration, Y. Amhis et al., *Averages of b-hadron, c-hadron and τ-lepton properties as of summer 2016*, Eur. Phys. J. **C 77** (2017) 895 [arXiv:1612.07233] [inSPIRE].

[10] HFLAV collaboration, *Summer 2018 update*, https://hflav-eos.web.cern.ch/hflav-eos/semi/summer18/RDRDs.html (2018).

[11] LHCb collaboration, *Test of lepton universality using $B^+ \to K^+\ell^+\ell^-$ decays*, Phys. Rev. Lett. **113** (2014) 151601 [arXiv:1406.6482] [inSPIRE].

[12] LHCb collaboration, *Test of lepton universality with $B^0 \to K^{*0}\ell^+\ell^-$ decays*, JHEP **08** (2017) 055 [arXiv:1705.05802] [inSPIRE].

[13] LHCb collaboration, *Angular analysis of the $B^0 \to K^{*0}\mu^+\mu^-$ decay using $3\,fb^{-1}$ of integrated luminosity*, JHEP **02** (2016) 104 [arXiv:1512.04442] [inSPIRE].

[14] LHCb collaboration, *Measurement of form-factor-independent observables in the decay $B^0 \to K^{*0}\mu^+\mu^-$*, Phys. Rev. Lett. **111** (2013) 191801 [arXiv:1308.1707] [inSPIRE].

[15] A. Datta, M. Duraisamy and D. Ghosh, *Diagnosing new physics in $b \to c\tau\nu_\tau$ decays in the light of the recent BaBar result*, Phys. Rev. **D 86** (2012) 034027 [arXiv:1206.3760] [inSPIRE].

[16] B. Bhattacharya, A. Datta, D. London and S. Shivashankara, *Simultaneous explanation of the R_K and $R(D^{(*)})$ puzzles*, Phys. Lett. **B 742** (2015) 370 [arXiv:1412.7164] [inSPIRE].

[17] R. Alonso, B. Grinstein and J. Martin Camalich, *Lepton universality violation and lepton flavor conservation in B-meson decays*, JHEP **10** (2015) 184 [arXiv:1505.05164] [inSPIRE].

[18] A. Greljo, G. Isidori and D. Marzocca, *On the breaking of lepton flavor universality in B decays*, JHEP **07** (2015) 142 [arXiv:1506.01705] [inSPIRE].

[19] L. Calibbi, A. Crivellin and T. Ota, *Effective field theory approach to $b \to s\ell\ell'$, $B \to K^*\nu\bar{\nu}$ and $B \to D^*\tau\nu$ with third generation couplings*, Phys. Rev. Lett. **115** (2015) 181801 [arXiv:1506.02661] [inSPIRE].

[20] M. Bauer and M. Neubert, *Minimal leptoquark explanation for the $R_{D^{(*)}}$, R_K and $(g-2)_g$ anomalies*, Phys. Rev. Lett. **116** (2016) 141802 [arXiv:1511.01900] [inSPIRE].

[21] S. Fajfer and N. Košnik, *Vector leptoquark resolution of R_K and $R_{D^{(*)}}$ puzzles*, Phys. Lett. **B 755** (2016) 270 [arXiv:1511.06024] [inSPIRE].

JHEP10(2018)092

[22] R. Barbieri, G. Isidori, A. Pattori and F. Senia, *Anomalies in B-decays and U(2) flavour symmetry*, *Eur. Phys. J.* **C 76** (2016) 67 [arXiv:1512.01560] [INSPIRE].

[23] D. Buttazzo, A. Greljo, G. Isidori and D. Marzocca, *Toward a coherent solution of diphoton and flavor anomalies*, *JHEP* **08** (2016) 035 [arXiv:1604.03940] [INSPIRE].

[24] D. Das, C. Hati, G. Kumar and N. Mahajan, *Towards a unified explanation of $R_{D^{(*)}}$, R_K and $(g-2)_\mu$ anomalies in a left-right model with leptoquarks*, *Phys. Rev.* **D 94** (2016) 055034 [arXiv:1605.06313] [INSPIRE].

[25] S.M. Boucenna et al., *Phenomenology of an* SU(2) × SU(2) × U(1) *model with lepton-flavour non-universality*, *JHEP* **12** (2016) 059 [arXiv:1608.01349] [INSPIRE].

[26] D. Bečirević, S. Fajfer, N. Košnik and O. Sumensari, *Leptoquark model to explain the B-physics anomalies, R_K and R_D*, *Phys. Rev.* **D 94** (2016) 115021 [arXiv:1608.08501] [INSPIRE].

[27] G. Hiller, D. Loose and K. Schönwald, *Leptoquark flavor patterns & B decay anomalies*, *JHEP* **12** (2016) 027 [arXiv:1609.08895] [INSPIRE].

[28] D. Bardhan, P. Byakti and D. Ghosh, *A closer look at the R_D and R_{D^*} anomalies*, *JHEP* **01** (2017) 125 [arXiv:1610.03038] [INSPIRE].

[29] B. Bhattacharya et al., *Simultaneous explanation of the R_K and $R_{D^{(*)}}$ puzzles: a model analysis*, *JHEP* **01** (2017) 015 [arXiv:1609.09078] [INSPIRE].

[30] R. Barbieri, C.W. Murphy and F. Senia, *B-decay anomalies in a composite leptoquark model*, *Eur. Phys. J.* **C 77** (2017) 8 [arXiv:1611.04930] [INSPIRE].

[31] D. Bečirević, N. Košnik, O. Sumensari and R. Zukanovich Funchal, *Palatable leptoquark scenarios for lepton flavor violation in exclusive $b \to s\ell_1\ell_2$ modes*, *JHEP* **11** (2016) 035 [arXiv:1608.07583] [INSPIRE].

[32] M. Bordone, G. Isidori and S. Trifinopoulos, *Semileptonic B-physics anomalies: a general EFT analysis within $U(2)^n$ flavor symmetry*, *Phys. Rev.* **D 96** (2017) 015038 [arXiv:1702.07238] [INSPIRE].

[33] E. Megias, M. Quirós and L. Salas, *Lepton-flavor universality violation in R_K and $R_{D^{(*)}}$ from warped space*, *JHEP* **07** (2017) 102 [arXiv:1703.06019] [INSPIRE].

[34] A. Crivellin, D. Müller and T. Ota, *Simultaneous explanation of $R(D^{(*)})$ and $b \to s\mu^+\mu^-$: the last scalar leptoquarks standing*, *JHEP* **09** (2017) 040 [arXiv:1703.09226] [INSPIRE].

[35] Y. Cai, J. Gargalionis, M.A. Schmidt and R.R. Volkas, *Reconsidering the One Leptoquark solution: flavor anomalies and neutrino mass*, *JHEP* **10** (2017) 047 [arXiv:1704.05849] [INSPIRE].

[36] W. Altmannshofer, P. Bhupal Dev and A. Soni, *$R_{D^{(*)}}$ anomaly: a possible hint for natural supersymmetry with R-parity violation*, *Phys. Rev.* **D 96** (2017) 095010 [arXiv:1704.06659] [INSPIRE].

[37] F. Sannino, P. Stangl, D.M. Straub and A.E. Thomsen, *Flavor physics and flavor anomalies in minimal fundamental partial compositeness*, *Phys. Rev.* **D 97** (2018) 115046 [arXiv:1712.07646] [INSPIRE].

[38] D. Buttazzo, A. Greljo, G. Isidori and D. Marzocca, *B-physics anomalies: a guide to combined explanations*, *JHEP* **11** (2017) 044 [arXiv:1706.07808] [INSPIRE].

JHEP10(2018)092

[39] A. Azatov, D. Bardhan, D. Ghosh, F. Sgarlata and E. Venturini, *Anatomy of $b \to c\tau\nu$ anomalies*, arXiv:1805.03209 [INSPIRE].

[40] J. Kumar, D. London and R. Watanabe, *Combined explanations of the $b \to s\mu^+\mu^-$ and $b \to c\tau^-\bar{\nu}$ anomalies: a general model analysis*, arXiv:1806.07403 [INSPIRE].

[41] D. Bečirević et al., *Scalar leptoquarks from grand unified theories to accommodate the B-physics anomalies*, Phys. Rev. **D 98** (2018) 055003 [arXiv:1806.05689] [INSPIRE].

[42] P. Asadi, M.R. Buckley and D. Shih, *It's all right(-handed neutrinos): a new W' model for the $R_{D^{(*)}}$ anomaly*, JHEP **09** (2018) 010 [arXiv:1804.04135] [INSPIRE].

[43] A. Greljo, D.J. Robinson, B. Shakya and J. Zupan, *$R(D^{(*)})$ from W' and right-handed neutrinos*, JHEP **09** (2018) 169 [arXiv:1804.04642] [INSPIRE].

[44] S. Fajfer, J.F. Kamenik, I. Nisandzic and J. Zupan, *Implications of lepton flavor universality violations in B decays*, Phys. Rev. Lett. **109** (2012) 161801 [arXiv:1206.1872] [INSPIRE].

[45] X.-G. He and G. Valencia, *B decays with τ leptons in nonuniversal left-right models*, Phys. Rev. **D 87** (2013) 014014 [arXiv:1211.0348] [INSPIRE].

[46] G. Cvetič, F. Halzen, C.S. Kim and S. Oh, *Anomalies in (semi)-leptonic B decays $B^\pm \to \tau^\pm\nu$, $B^\pm \to D\tau^\pm\nu$ and $B^\pm \to D^*\tau^\pm\nu$ and possible resolution with sterile neutrino*, Chin. Phys. **C 41** (2017) 113102 [arXiv:1702.04335] [INSPIRE].

[47] S. Fraser et al., *Towards a viable scalar interpretation of $R_{D^{(*)}}$*, Phys. Rev. **D 98** (2018) 035016 [arXiv:1805.08189] [INSPIRE].

[48] R.N. Mohapatra, *Mechanism for understanding small neutrino mass in superstring theories*, Phys. Rev. Lett. **56** (1986) 561 [INSPIRE].

[49] R.N. Mohapatra and J.W.F. Valle, *Neutrino mass and baryon number nonconservation in superstring models*, Phys. Rev. **D 34** (1986) 1642 [INSPIRE].

[50] A.G. Dias et al., *A simple realization of the inverse seesaw mechanism*, Phys. Rev. **D 86** (2012) 035007 [arXiv:1206.2590] [INSPIRE].

[51] D.J. Robinson, B. Shakya and J. Zupan, *Right-handed neutrinos and $R(D^{(*)})$*, arXiv:1807.04753 [INSPIRE].

[52] R. Barbieri and A. Tesi, *B-decay anomalies in Pati-Salam* SU(4), Eur. Phys. J. **C 78** (2018) 193 [arXiv:1712.06844] [INSPIRE].

[53] J.M. Cline, *B decay anomalies and dark matter from vectorlike confinement*, Phys. Rev. **D 97** (2018) 015013 [arXiv:1710.02140] [INSPIRE].

[54] N. Assad, B. Fornal and B. Grinstein, *Baryon number and lepton universality violation in leptoquark and diquark models*, Phys. Lett. **B 777** (2018) 324 [arXiv:1708.06350] [INSPIRE].

[55] L. Calibbi, A. Crivellin and T. Li, *A model of vector leptoquarks in view of the B-physics anomalies*, arXiv:1709.00692 [INSPIRE].

[56] L. Di Luzio, A. Greljo and M. Nardecchia, *Gauge leptoquark as the origin of B-physics anomalies*, Phys. Rev. **D 96** (2017) 115011 [arXiv:1708.08450] [INSPIRE].

[57] M. Bordone, C. Cornella, J. Fuentes-Martin and G. Isidori, *A three-site gauge model for flavor hierarchies and flavor anomalies*, Phys. Lett. **B 779** (2018) 317 [arXiv:1712.01368] [INSPIRE].

JHEP10(2018)092

[58] A. Greljo and B.A. Stefanek, *Third family quark–lepton unification at the TeV scale*, Phys. Lett. **B 782** (2018) 131 [arXiv:1802.04274] [INSPIRE].

[59] M. Blanke and A. Crivellin, *B meson anomalies in a Pati-Salam model within the Randall-Sundrum background*, Phys. Rev. Lett. **121** (2018) 011801 [arXiv:1801.07256] [INSPIRE].

[60] M. Bordone, C. Cornella, J. Fuentes-Martín and G. Isidori, *Low-energy signatures of the* PS^3 *model: from B-physics anomalies to LFV*, arXiv:1805.09328 [INSPIRE].

[61] W. Altmannshofer, P. Stangl and D.M. Straub, *Interpreting hints for lepton flavor universality violation*, Phys. Rev. **D 96** (2017) 055008 [arXiv:1704.05435] [INSPIRE].

[62] S. Descotes-Genon, L. Hofer, J. Matias and J. Virto, *Global analysis of* $b \to s\ell\ell$ *anomalies*, JHEP **06** (2016) 092 [arXiv:1510.04239] [INSPIRE].

[63] G. D'Amico et al., *Flavour anomalies after the* R_{K^*} *measurement*, JHEP **09** (2017) 010 [arXiv:1704.05438] [INSPIRE].

[64] B. Capdevila et al., *Patterns of new physics in* $b \to s\ell^+\ell^-$ *transitions in the light of recent data*, JHEP **01** (2018) 093 [arXiv:1704.05340] [INSPIRE].

[65] M. Ciuchini et al., *On flavourful easter eggs for new physics hunger and lepton flavour universality violation*, Eur. Phys. J. **C 77** (2017) 688 [arXiv:1704.05447] [INSPIRE].

[66] D. Ghosh, *Explaining the* R_K *and* R_{K^*} *anomalies*, Eur. Phys. J. **C 77** (2017) 694 [arXiv:1704.06240] [INSPIRE].

[67] G. Hiller and I. Nisandzic, R_K *and* R_{K^*} *beyond the standard model*, Phys. Rev. **D 96** (2017) 035003 [arXiv:1704.05444] [INSPIRE].

[68] D. Bardhan, P. Byakti and D. Ghosh, *Role of tensor operators in* R_K *and* R_{K^*}, Phys. Lett. **B 773** (2017) 505 [arXiv:1705.09305] [INSPIRE].

[69] R. Alonso, B. Grinstein and J. Martin Camalich, *Lifetime of* B_c^- *constrains explanations for anomalies in* $B \to D^{(*)}\tau\nu$, Phys. Rev. Lett. **118** (2017) 081802 [arXiv:1611.06676] [INSPIRE].

[70] S. Aoki et al., *Review of lattice results concerning low-energy particle physics*, Eur. Phys. J. **C 77** (2017) 112 [arXiv:1607.00299] [INSPIRE].

[71] Particle Data Group collaboration, M. Tanabashi et al., *Review of Particle Physics*, Phys. Rev. **D 98** (2018) 030001.

[72] D. Bečirević, O. Sumensari and R. Zukanovich Funchal, *Lepton flavor violation in exclusive* $b \to s$ *decays*, Eur. Phys. J. **C 76** (2016) 134 [arXiv:1602.00881] [INSPIRE].

[73] BaBar collaboration, J.P. Lees et al., *A search for the decay modes* $B^{+-} \to h^{+-}\tau^{+-}l$, Phys. Rev. **D 86** (2012) 012004 [arXiv:1204.2852] [INSPIRE].

[74] F. Feruglio, P. Paradisi and A. Pattori, *Revisiting lepton flavor universality in B decays*, Phys. Rev. Lett. **118** (2017) 011801 [arXiv:1606.00524] [INSPIRE].

[75] F. Feruglio, P. Paradisi and A. Pattori, *On the importance of electroweak corrections for B anomalies*, JHEP **09** (2017) 061 [arXiv:1705.00929] [INSPIRE].

[76] C. Cornella, F. Feruglio and P. Paradisi, *Low-energy effects of lepton flavour universality violation*, arXiv:1803.00945 [INSPIRE].

JHEP10(2018)092

[77] SLD Electroweak Group, DELPHI, ALEPH, SLD, SLD Heavy Flavour Group, OPAL, LEP Electroweak Working Group, L3 collaboration, S. Schael et al., *Precision electroweak measurements on the Z resonance*, *Phys. Rept.* **427** (2006) 257 [hep-ex/0509008] [INSPIRE].

[78] B. Gripaios, *Composite leptoquarks at the LHC*, *JHEP* **02** (2010) 045 [arXiv:0910.1789] [INSPIRE].

[79] Y. Sakaki, M. Tanaka, A. Tayduganov and R. Watanabe, *Testing leptoquark models in* $\bar{B} \to D^{(*)}\tau\bar{\nu}$, *Phys. Rev.* **D 88** (2013) 094012 [arXiv:1309.0301] [INSPIRE].

[80] G. Hiller and M. Schmaltz, R_K *and future* $b \to s\ell\ell$ *physics beyond the standard model opportunities*, *Phys. Rev.* **D 90** (2014) 054014 [arXiv:1408.1627] [INSPIRE].

[81] B. Gripaios, M. Nardecchia and S.A. Renner, *Composite leptoquarks and anomalies in B-meson decays*, *JHEP* **05** (2015) 006 [arXiv:1412.1791] [INSPIRE].

[82] I. Doršner, S. Fajfer, D.A. Faroughy and N. Košnik, *The role of the* S_3 *GUT leptoquark in flavor universality and collider searches*, arXiv:1706.07779 [INSPIRE].

[83] S. Fajfer, N. Košnik and L. Vale Silva, *Footprints of leptoquarks: from* $R_{K^{(*)}}$ *to* $K \to \pi\nu\bar{\nu}$, *Eur. Phys. J.* **C 78** (2018) 275 [arXiv:1802.00786] [INSPIRE].

[84] D. Marzocca, *Addressing the B-physics anomalies in a fundamental composite Higgs Model*, *JHEP* **07** (2018) 121 [arXiv:1803.10972] [INSPIRE].

[85] A.G. Akeroyd and C.-H. Chen, *Constraint on the branching ratio of* $B_c \to \tau\bar{\nu}$ *from LEP1 and consequences for* $R(D^{(*)})$ *anomaly*, *Phys. Rev.* **D 96** (2017) 075011 [arXiv:1708.04072] [INSPIRE].

[86] M. Jung and D.M. Straub, *Constraining new physics in* $b \to c\ell\nu$ *transitions*, arXiv:1801.01112 [INSPIRE].

[87] UTfit collaboration, *Latest results from UTfit*, http://www.utfit.org/UTfit/ (2016).

[88] L. Di Luzio, M. Kirk and A. Lenz, *Updated* B_s*-mixing constraints on new physics models for* $b \to s\ell^+\ell^-$ *anomalies*, *Phys. Rev.* **D 97** (2018) 095035 [arXiv:1712.06572] [INSPIRE].

[89] Fermilab Lattice, MILC collaboration, A. Bazavov et al., $B^0_{(s)}$*-mixing matrix elements from lattice QCD for the Standard Model and beyond*, *Phys. Rev.* **D 93** (2016) 113016 [arXiv:1602.03560] [INSPIRE].

[90] M. Blanke and A.J. Buras, *Universal Unitarity Triangle 2016 and the tension between* $\Delta M_{s,d}$ *and* ε_K *in CMFV models*, *Eur. Phys. J.* **C 76** (2016) 197 [arXiv:1602.04020] [INSPIRE].

[91] I. Doršner and A. Greljo, *Leptoquark toolbox for precision collider studies*, *JHEP* **05** (2018) 126 [arXiv:1801.07641] [INSPIRE].

[92] J. Alwall et al., *The automated computation of tree-level and next-to-leading order differential cross sections and their matching to parton shower simulations*, *JHEP* **07** (2014) 079 [arXiv:1405.0301] [INSPIRE].

[93] C. Degrande et al., *UFO — The Universal FeynRules Output*, *Comput. Phys. Commun.* **183** (2012) 1201 [arXiv:1108.2040] [INSPIRE].

[94] CMS collaboration, *Search for third-generation scalar leptoquarks and heavy right-handed neutrinos in final states with two tau leptons and two jets in proton-proton collisions at* $\sqrt{s} = 13$ *TeV*, *JHEP* **07** (2017) 121 [arXiv:1703.03995] [INSPIRE].

JHEP10(2018)092

[95] CMS collaboration, *Search for heavy neutrinos and third-generation leptoquarks in final states with two hadronically decaying τ leptons and two jets in proton-proton collisions at $\sqrt{s} = 13$ TeV*, CMS-PAS-EXO-17-016 (2018).

[96] ATLAS collaboration, *Search for squarks and gluinos in final states with jets and missing transverse momentum using $36\,fb^{-1}$ of $\sqrt{s} = 13$ TeV pp collision data with the ATLAS detector*, *Phys. Rev.* **D 97** (2018) 112001 [arXiv:1712.02332] [INSPIRE].

[97] CMS collaboration, *Constraints on models of scalar and vector leptoquarks decaying to a quark and a neutrino at $\sqrt{s} = 13$ TeV*, *Phys. Rev.* **D 98** (2018) 032005 [arXiv:1805.10228] [INSPIRE].

[98] ATLAS collaboration, *Search for high-mass resonances decaying to $\tau\nu$ in pp collisions at $\sqrt{s} = 13$ TeV with the ATLAS detector*, *Phys. Rev. Lett.* **120** (2018) 161802 [arXiv:1801.06992] [INSPIRE].

[99] CMS collaboration, *Search for new physics in final states with an energetic jet or a hadronically decaying W or Z boson and transverse momentum imbalance at $\sqrt{s} = 13$ TeV*, *Phys. Rev.* **D 97** (2018) 092005 [arXiv:1712.02345] [INSPIRE].

[100] D.A. Faroughy, A. Greljo and J.F. Kamenik, *Confronting lepton flavor universality violation in B decays with high-p_T tau lepton searches at LHC*, *Phys. Lett.* **B 764** (2017) 126 [arXiv:1609.07138] [INSPIRE].

[101] CMS collaboration, *Identification of heavy-flavour jets with the CMS detector in pp collisions at 13 TeV*, 2018 *JINST* **13** P05011 [arXiv:1712.07158] [INSPIRE].

[102] M. Drewes and B. Garbrecht, *Combining experimental and cosmological constraints on heavy neutrinos*, *Nucl. Phys.* **B 921** (2017) 250 [arXiv:1502.00477] [INSPIRE].

[103] M. Drewes, J. Hajer, J. Klaric and G. Lanfranchi, *NA62 sensitivity to heavy neutral leptons in the low scale seesaw model*, *JHEP* **07** (2018) 105 [arXiv:1801.04207] [INSPIRE].

[104] P. Ballett, T. Boschi and S. Pascoli, *Searching for MeV-scale neutrinos with the DUNE near detector*, talk given at *Prospects in Neutrino Physics (NuPhys2017)*, December 20–22, London, U.K. (2018), arXiv:1803.10824 [INSPIRE].

[105] S.S. Gershtein and Ya.B. Zeldovich, *Rest mass of muonic neutrino and cosmology*, *JETP Lett.* **4** (1966) 120 [INSPIRE].

[106] R. Cowsik and J. McClelland, *An upper limit on the neutrino rest mass*, *Phys. Rev. Lett.* **29** (1972) 669 [INSPIRE].

[107] A. Boyarsky, J. Lesgourgues, O. Ruchayskiy and M. Viel, *Lyman-α constraints on warm and on warm-plus-cold dark matter models*, *JCAP* **05** (2009) 012 [arXiv:0812.0010] [INSPIRE].

[108] G. Steigman, *Equivalent neutrinos, light WIMPs and the chimera of dark radiation*, *Phys. Rev.* **D 87** (2013) 103517 [arXiv:1303.0049] [INSPIRE].

[109] Planck collaboration, P.A.R. Ade et al., *Planck 2015 results. XIII. Cosmological parameters*, *Astron. Astrophys.* **594** (2016) A13 [arXiv:1502.01589] [INSPIRE].

[110] R.J. Scherrer and M.S. Turner, *Decaying particles do not heat up the universe*, *Phys. Rev.* **D 31** (1985) 681 [INSPIRE].

[111] E.W. Kolb and M.S. Turner, *The early universe*, *Front. Phys.* **69** (1990) 1 [INSPIRE].

JHEP10(2018)092

[112] M. Nemevšek, G. Senjanović and Y. Zhang, *Warm dark matter in low scale left-right theory*, *JCAP* **07** (2012) 006 [arXiv:1205.0844] [INSPIRE].

[113] S.F. King and A. Merle, *Warm dark matter from keVins*, *JCAP* **08** (2012) 016 [arXiv:1205.0551] [INSPIRE].

[114] F. Bezrukov, H. Hettmansperger and M. Lindner, *keV sterile neutrino dark matter in gauge extensions of the standard model*, *Phys. Rev.* **D 81** (2010) 085032 [arXiv:0912.4415] [INSPIRE].

[115] R. Essig et al., *Constraining light dark matter with diffuse X-ray and gamma-ray observations*, *JHEP* **11** (2013) 193 [arXiv:1309.4091] [INSPIRE].

[116] A. Boyarsky et al., *Sterile neutrino dark matter*, arXiv:1807.07938 [INSPIRE].

[117] S. Davidson, E. Nardi and Y. Nir, *Leptogenesis*, *Phys. Rept.* **466** (2008) 105 [arXiv:0802.2962] [INSPIRE].

JHEP10(2018)092